Acoustic Fresnel Lens

to focus ultrasound for *in vitro* neuromodulation

Reka Savundranayagam

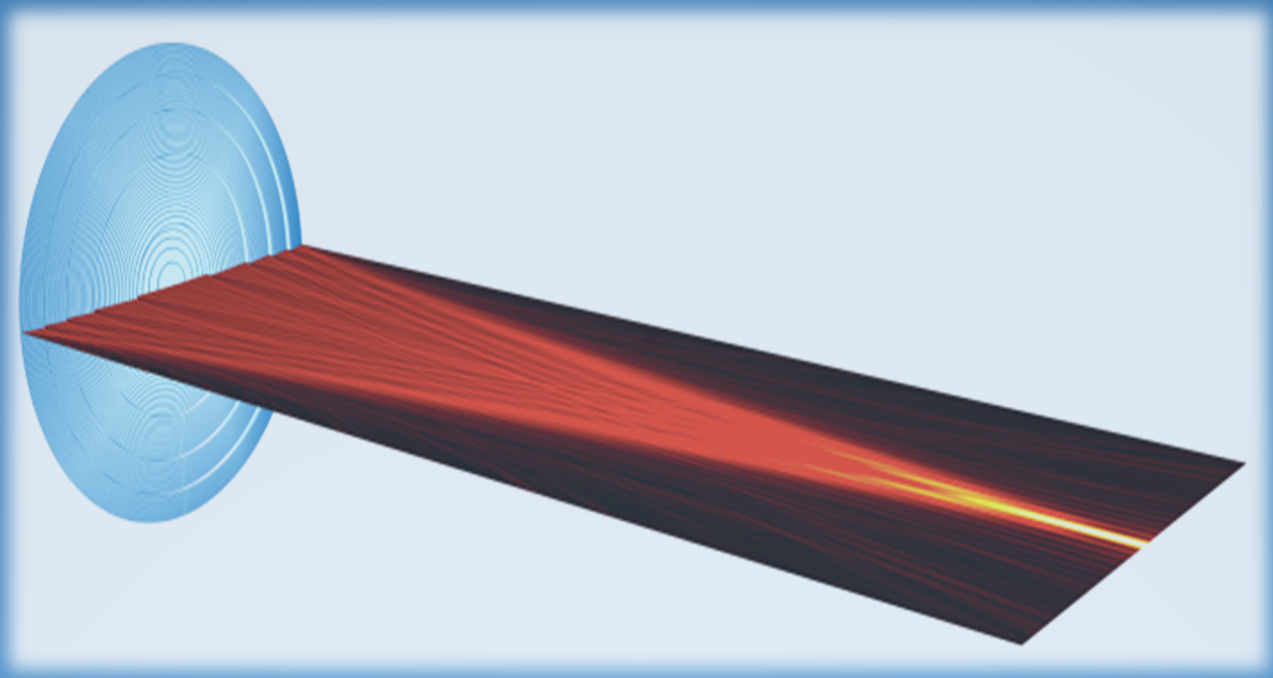

TU Delft

Acoustic Fresnel Lens

to focus ultrasound for *in vitro* neuromodulation

By

Reka Savundranayagam
4452577

A thesis submitted in partial fulfilment of the requirements for the degree of

Master of Science
in Biomedical Engineering
Track: Medical Devices and Bioelectronics

at the Delft University of Technology

Supervisor:	Dr. T.M.L. Costa
Thesis committee:	Dr. T.M.L. Costa
	Dr. C.M.F. Viellard-Boutry
	Ir. G. Wardhana

TU Delft

Preface

As a Biomedical Engineering student with a background in Technical Medicine, I have always been fascinated by the potential of medical technologies to improve human health and quality of life. In this thesis, I explore the use of acoustic Fresnel lenses to focus ultrasound for *in vitro* neuromodulation purposes.

My interest in ultrasound was sparked by a course I took during my master, called 'Themes in Biomedical Electronics', where I was first introduced to the topic ultrasound neuromodulation by Dr. Tiago Costa. I was assigned to write an essay on ultrasound neuromodulation and it was through this assignment that my interest in this field truly took hold. I was fascinated by the prospect of using ultrasound to non-invasively modulate neural activity and realized that this could have far reaching possibilities in the treatment of a variety of neurological disorders. Two years after the assignment, I approached Dr. Tiago Costa to inquire about possible Master Thesis projects and I was fortunate enough to be given the opportunity to work on a project in the area of focused ultrasound.

I would like to thank Dr. Tiago Costa for his guidance throughout my master's thesis journey. The provided flexibility is much appreciated and his way of approaching obstacles with a positive and solution-oriented attitude has been an inspiration to me. The weekly group meetings he arranged gave the students the possibility to discuss problems and to get new insights to continue their work. Besides his outstanding expertise in science, he also possesses a great passion for ping pong. As far as I can remember, he was topping the ranking list of the 16th floor for the past year. I really hope that one day his contributions to the exciting field of miniaturized devices for biomedical applications are implemented in the clinical practice.

Then, I would like to thank ir. Gandhi Wardhana. He was my daily supervisor and has taught me everything in the cleanroom. Gandhi's innate curiosity and passion for understanding the workings of even the smallest things make him a true engineer. His creative mind constantly explores possibilities and he never shies away from a challenge. The past year has been an inspiring learning experience, as I have gained much practical and theoretical knowledge from Gandhi. His hard-working nature and exceptional ability to explain complex concepts clearly make him a valuable asset in any team. Not only is Gandhi an excellent scientist, his kind and helpful personality makes him a valued friend. Our conversations always covered a wide range of topics and Gandhi's insightful and well-reasoned arguments make him a great conversationalist.

I would like to thank my family. My parents always motivated and encouraged me to go after my goals and to reach my full potential. They are very loving and caring, always putting in extra effort to make sure I am comfortable. Whenever I visited my parents, their delicious home-cooked meals provided me nourishment to fuel my academic pursuits. My younger brother's (sometimes too) relaxed and carefree lifestyle was a reassuring presence during challenging times, reminding me to take a step back and approach problems with a lighter perspective.

Lastly, I am deeply grateful for my caring boyfriend who is always by my side. He was a constant source of support, always lending a listening ear and providing realistic advice. His sense of humor and infectious laughter never fail to bring a smile to my face. He not only makes every day filled with happiness, he also gives me all the space to chase my dreams. I am thankful for having such a genuine and kind-hearted person in my life who brings so much positivity into it.

With gratitude and appreciation expressed, it's now time to delve into the heart of this thesis. By presenting this work, I hope I can contribute to the growing body of knowledge in the field of focused ultrasound and provide a foundation for future research.

Abstract

In vitro neuromodulation studies play a crucial role in understanding the underlying interaction mechanisms between cells and ultrasound, which is important in the development of new therapies for various neurological disorders. Acoustic focusing, the ability to focus ultrasound at a specific focal length with high spatial resolution, provides a precise and effective way to stimulate cell cultures. In this way, researchers are able to stimulate specific cells or regions within a cell culture, leading to a better understanding of cellular behaviour and responses to ultrasound stimulation.

This thesis focuses on designing and developing a microfabricated acoustic Fresnel lens to focus ultrasound at a pre-determined focal length to fit into currently used Microelectrode Array (MEA) devices. Polydimethylsiloxane (PDMS) is used as lens material and microfabrication technologies are employed for the fabrication of a silicon mold. Experimental measurements have been conducted in an underwater configuration to evaluate the performance of the acoustic lens. The research highlights the potential of using acoustic Fresnel lenses on ultrasound transducers for *in vitro* neuromodulation. The results of the study demonstrate their capability to effectively focus ultrasound waves at the desired focal length. This advancement has significant implications for the field of *in vitro* neuromodulation, as it offers a cost-effective and promising method for achieving more accurate stimulation of cell cultures and for studying the impact of various acoustic parameters on cells.

Contents

List of Abbreviations

Abbreviation	Definition
2D	2 dimensional
3D	3 dimensional
ALS	amyotrophic lateral sclerosis
Al	aluminium
BHF	buffered hydrofluoric acid
CMOS	complementary metal oxide semiconductor
CMUT	capacitive micromachined ultrasound transducer
Cr	chromium
DC	direct current
DI	deionized water
DRIE	deep reactive ion etching
EVA	experimental visual acoustics, in-house developed MATLAB Software
FEA	finite element analysis
FPZP	Fresnel phase zone plate
FUS	focused ultrasound
FWHM	full width at half maximum
FZP	Fresnel Zone Plate
HIFU	high intensity focused ultrasound
ICM	injection compression moulding
IM	injection moulding
I_{spta}	spatial peak temporal average intensity
I_{sptp}	temporal peak acoustic intensity
I_{sspa}	spatial peak average intensity
LIFU	low intensity focused ultrasound
MEA	multielectrode array
MEMS	microelectromechanical systems
MUT	micromachined ultrasound transducer
PDMS	polydimethylsiloxane, thermoset material
PECVD	plasma enhanced chemical vapor deposition
PFTE	polytetrafluoroethylene (Teflon), fluoropolymer material
PMMA	polymethylmethacrylate, thermoplastic material
PMN-PT	lead magnesium niobate-lead titanate, piezoelectric material
PMUT	piezoelectric micromachined ultrasound transducer
PZT	lead zirconate titanate, piezoelectric material
Q	mechanical quality factor
SPL	spatial pulse length
SSP	single side polished
SiO_2	silicon dioxide
Ti	titanium
NLOF	negative photoresist

1. Introduction

Ultrasound is well-known for its diagnostic medical imaging purposes. The therapeutic use of ultrasound is currently being investigated. Globally millions of people get affected by neurodegenerative diseases, such as Alzheimer disease, Parkinson disease and Amyotrophic Lateral Sclerosis (ALS) and by non-neurodegenerative diseases, such as epilepsy and depressive disorders. At present, there is no cure for (non) neurodegenerative diseases. The available treatments are used to suppress symptoms or to prevent progression of the disease. The first option of treatment is often pharmaceuticals, but these have a lot of side-effects. Another option is the use of electroceuticals or implantable electrodes, which are both highly invasive. There is a need in finding a treatment that is minimally invasive and targets the tissue with high spatial resolution to reduce side effects.

Focused ultrasound (FUS) is the tool towards ultrasound neuromodulation with the goal to cure or prevent neurological diseases. FUS uses beams of ultrasound energy with high precision to target different tissues in the body and is considered a minimally invasive treatment. High-intensity focused ultrasound (HIFU) makes use of frequencies that generate a localized high temperature rise, inducing thermal ablation for therapeutic purposes [1]. Low intensity focused ultrasound (LIFU) operates at frequencies that lead to low energy delivery in the tissue and produces mechanical effects, such as structural deformations of cell membranes and increased cell permeability, without inducing thermal rises or tissue damage [1,2]. Therefore, low-intensity ultrasound is rapidly emerging and a good candidate for different therapeutic modalities, such as bone fracture healing, drug delivery and non-invasive neuromodulation [3].

1.1. Ultrasound neuromodulation – the need for advanced transducers for *in vitro* studies

Different *in vitro* and *in vivo* studies showed that LIFU modulates the excitability of neuronal cells with high spatial resolution and without the need for invasive processes [1,2,4], whereas commonly used electrical brain stimulation techniques often suffer from poor spatial resolution or include invasive treatments. In LIFU, the stimulation parameters, such as acoustic intensity and exposure time, can be altered to induce activation or suppression of neuronal activity. In addition, LIFU is used for stimulating different *in vitro* cell cultures to promote cell proliferation, differentiation and viability [3,5]. Ultrasound neuromodulation is independent of voltage-gated ion channels in the neuronal cell membrane. This is in contrast with electrical stimulation, which depends on the expression of specific ion channels [6]. For instance, neuronal progenitor cells may not have fully developed voltage-gated ion channels, making ultrasound stimulation a potential candidate to induce differentiation from neural progenitor cells into active neurons. *In vitro* studies are often the first indication to determine if a LIFU therapeutic treatment is completely safe, controllable and repeatable. These aspects are essential to consider before a LIFU-based treatment is implemented in clinical practice.

Researching the effects of ultrasound at the cellular level is crucial for understanding the interaction mechanisms between LIFU and cells. The possible mechanisms evoked by ultrasound are direct and indirect mechanical effects, including radiation force, membrane cavitation and redistribution of signaling molecules [7]. As appointed, LIFU does not result in transforming ultrasound energy into thermal rises. However, heating of the transducer can influence the LIFU induced stimulation of *in vitro* cell cultures. Other confounding factors are

non-uniform cell stimulation, distortions in the transmitted ultrasound waves and reflection through the petri dish containing cell cultures and the formation of standing waves [7]. Such factors could alter the outcomes of *in vitro* ultrasound experiments and thus, affecting the reproducibility of the experiments. Moreover, it influences the consistency of the acoustic parameters, e.g. duration, frequency and duty cycle. To overcome these limitations, a LIFU-micro platform compatible with *in vitro* cell cultures needs to be designed for uniform stimulation of the cells in order to study and control the mechanical effects induced by LIFU.

Another important aspect to be taken into consideration is acoustic focusing, which is essential for focusing the ultrasound waves at the *in vitro* cells being studied. This allows researchers to study the effects of different acoustic parameters on cells and to understand how stimulated cells behave compared to the surrounding cells. Acoustic focusing can be achieved by implementing acoustic lenses in ultrasound transducers. To avoid distortion of the energy distribution through the lens, it is important to include the transducer parameters, such as frequency and wavelength, in the design of the acoustic lens.

The goal of the present study, in a step towards modulating neuronal networks using ultrasound, is to design and fabricate an acoustic lens that can be placed on the surface of an ultrasound transducer to concentrate the acoustic waves at the primary focus for modulating *in vitro* neuronal cells. The main focus of the research is achieving the pre-determined focal length, a small focal spot size and high intensities at the focal spot in order to assess the performance of the acoustic lens.

1.2. Organization of the thesis

This thesis is divided into different chapters. Chapter 2 highlights relevant literature, comparing the different types of ultrasound transducers and explaining different acoustic focusing mechanisms with the focus on acoustic Fresnel lenses. Based on the findings from the literature study, a research plan is defined at the end of the chapter. The methodologies used for conducting this study are described in Chapter 3. First, simulations are performed to assess the performance of the designed acoustic lens. This is followed by describing the microfabrication techniques employed for producing the acoustic Fresnel lenses and other components required for the assembly process of the ultrasound transducer. At last, the experimental measurement set up is demonstrated. Chapter 4 provides the results of the experimental measurements to assess the performance of the fabricated acoustic Fresnel lens. A comparison is made for the ultrasound transducer with and without acoustic lens. The different focal lengths and focal spot sizes are derived from the measured acoustic intensity profiles. The research findings and the limitations of the study are discussed in Chapter 5. Furthermore, different recommendations for improvements are described. Finally, in Chapter 6, concluding remarks and directions for potential future work are pointed out.

2. Literature review

This chapter presents a literature study to gain information from previous studies pertaining to the question: How to design and manufacture an acoustic lens to place on the surface of an ultrasound transducer for focusing ultrasound to modulate *in vitro* neural cells? Section 2.1 gives an overview of ultrasound transducers in general, making a distinction between bulk piezoelectric transducers and micromachined ultrasound transducers. Section 2.2 elaborates on the ultrasound transducers characteristics for *in vitro* neuromodulation. Section 2.3 focuses on the design and fabrication of acoustic lenses.

2.1. Ultrasound transducers

2.1.1. Conventional Bulk Piezoelectric Transducers

Ultrasound transducers consist of piezoelectric crystals and convert mechanical vibrations into electrical energy or *vice versa*. When mechanical vibrations lead to a deformation of the crystal, and therefore, a disbalance of charges, an electrical voltage is generated, which can be detected. Contrariwise, when an electrical voltage is applied across the crystal, a mechanical effect or deformation of the crystal structure occurs. Two types of ultrasound transducers exist, the conventional bulk ceramic transducer and the micromachined ultrasound transducer (MUT). Bulk ceramic transducers are based on piezoelectric ceramics, such as lead zirconate titanate (PZT), and operate in the thickness direction for different applications. The operating frequency is determined by the speed of sound in the layer and the thickness of the piezoelectric layer; for transducers operating in the frequency range of 1 – 10 MHz, the thickness of the piezoelectric layer is 100 - 1000 μm [8,9]. In order to operate at the resonance frequency of a transducer, the optimal piezoelectric layer thickness is equal to half the wavelength [10]. Transducers that operate at high frequencies require thinner piezoelectric layers compared to transducers that operate at low frequencies.

In Figure 1, a single-element ultrasonic piezoelectric transducer is shown. The piezoelectric material is located between the top and bottom electrode. Since the waves emitted by the piezoelectric transducer propagate in the surrounding medium, it requires an impedance matching layer to compensate for the acoustic impedance mismatch between the piezoelectric transducer and the medium [11,12]. Acoustic impedance matching of the transducer and surrounding medium is of importance for increasing the transmittance of acoustic waves. The matching layer consists of materials with acoustic impedances similar to that of the medium and the piezoelectric layer. The optimal thickness of the matching layer is equal to ¼ of the wavelength, which is determined by the resonance frequency of the transducer and the speed of sound in the matching layer [10]. Furthermore, in case of imaging transducers, a backing layer is required to increase the bandwidth by absorbing ultrasound waves propagating backward from the piezoelectric element, which can cause undesired noise [11,12]. The backing layer absorbs backward emitted sound waves and dampens the vibrations of the transducer, resulting in an ultrasound pulse with a short spatial pulse length (SPL) [10]. Decreasing the pulse length improves the axial resolution. Furthermore, the backing layer broadens the frequency bandwidth. Highly damped transducers have a short SPL and are able to operate at frequencies above and below the central frequency.

The piezoelectric elements of an ultrasound transducer are arranged in linear arrays. A linear array transducer operates by simultaneously activating a subset of the piezoelectric elements and requires physically moving of the transducer for steering and focusing the ultrasound beam [10]. Furthermore, the focal length of a linear array transducer is fixed and is determined by the transducer diameter, the center frequency and the acoustic lens [10]. Linear array bulk ceramic transducers are relatively large in size because the fabrication requires dicing of the piezoelectric ceramics by diamond blades. The size of the diamond blades limits the minimum gap between the piezoelectric elements [8,13]. Therefore, a reduction in size is also limited. The large dimensions limit bulk ceramic transducers to be used for applications in small devices. Furthermore, piezoceramics are characterized by a high acoustic impedance, making them difficult to match with media [9,13]. These limitations necessitated the use of MEMS technology. Micromachined ultrasound transducers (MUTs), utilizing thin films, have better acoustic impedance matching, larger bandwidth and more possibilities for array design and CMOS-integration compared to conventional bulk ultrasound transducers [13,14]. The MUTs are categorized into two types: the capacitive micromachined ultrasound transducer (CMUT) and the piezoelectric micromachined ultrasonic transducer (PMUT). The two types of MUTs will be discussed in detail in the following sections.

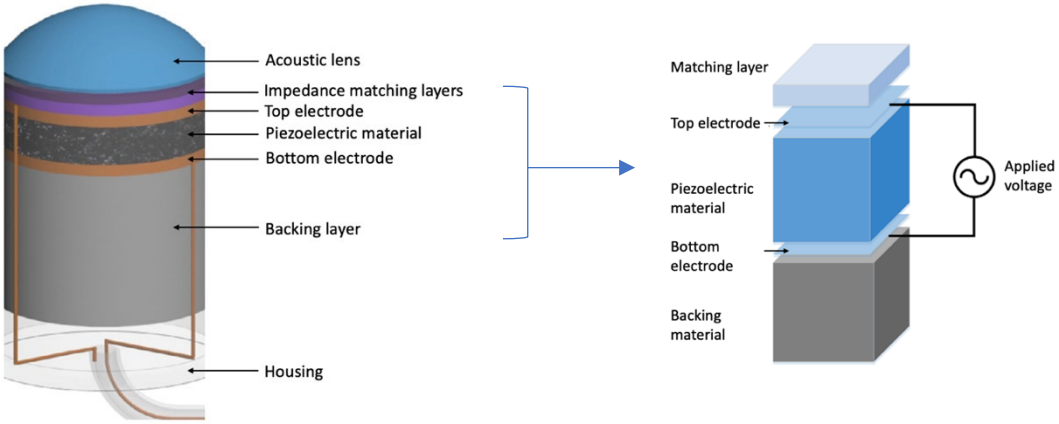

Figure 1– Schematic view of a single-element ultrasonic piezoelectric transducer (adapted from Ref. [12])

2.1.2. Capacitive Micromachined Ultrasonic Transducer (CMUT)

CMUTs are electrostatic transducers based on silicon. CMUTs consist of a movable top electrode (membrane) and a fixed bottom electrode, as shown in Figure 2. For signal detection, a direct current (DC) bias voltage is applied between the two electrodes. When an alternating voltage is applied to the biased top electrode, an electrostatic force is modulated, which results in vibration of the top electrode and generation of ultrasound waves [10, 16]. Conversely, when the top electrode is subjected to ultrasound waves, a change in capacitance occurs, generating a detectable electrical current. The amplitude of the current is determined by the frequency of the incident ultrasound wave, the bias voltage and the capacitance of the device [16]. The principles of operation can be categorized into three modes: conventional, collapse and collapse back [12,17].

In the conventional operation mode, the DC bias voltage of the CMUT approaches the collapse voltage and the sum of the DC bias voltage and the alternating voltage is set to a pre-calculated value so that the membrane does not touch the substrate [17]. Increasing the bias voltage will lead to the membrane collapsing onto the bottom electrode, since the electrostatic

force will become greater than the mechanical force. When the membrane makes contact with the bottom electrode and the bias voltage is decreased to a voltage that is lower than the collapse voltage, the membrane recovers back to its original shape and to the position at the voltage applied before collapse voltage [17].

For the collapse operation mode, the DC bias voltage is larger than the snapback voltage, which results in constant contact between the membrane and the bottom electrode. In the collapse back operation mode, the DC bias voltage is set between the collapse and snapback voltages, causing the center of the membrane to be in contact with the bottom electrode [18]. Studies have shown that the collapse mode and the collapse back mode have a high coupling coefficient compared to the conventional mode [12,17,18]. The micromachining technology enables the distance between the two electrodes to be less than a micron, causing high electric fields in the gap [10,19].

One of the main advantages of CMUTs compared to bulk transducers is the wide frequency bandwidth due to better acoustic matching with the medium [16]. Other well-known advantages of CMUTs are improved resolution and the ability to integrate with electronic circuits by the use of CMOS-compatible materials, such as silicon nitride [10,16]. The CMUT transducer makes use of high biasing voltages to operate closely to the pull-in voltage. This is required to maximize the coupling coefficient and to acquire optimal bandwidth and sensitivity [8]. In addition, the stroke of the top electrode, which is required for generating acoustic output, is limited by the vacuum gap [10,16]. Piezoelectric micromachined ultrasonic transducers (PMUTs) have several advantages over CMUTs, such as the elimination of high biasing voltages and operating in the low frequency range [20]. The total displacement of PMUTs does not depend on the vacuum gap and the design of PMUTs will not be limited by the buildup of charge and dielectric breakdown [20]. Overall, PMUTs are more suitable for cell stimulation compared to CMUTs because of the low-frequency range PMUTs operate in.

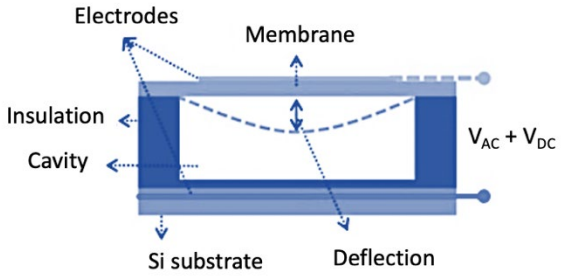

Figure 2 – Schematic view of a capacitive micromachined ultrasonic transducer (CMUT) consisting of a membrane with top electrode and a fixed bottom electrode (adapted from Ref. [15]).

2.1.3. Piezoelectric Micromachined Ultrasonic Transducer (PMUT)

In Figure 3, a PZT-based PMUT is shown. PMUTs generally consist of passive layers, such as silicon (Si) and silicon dioxide (SiO2), and piezoelectric layers made from lead zirconate titanate (PZT), zinc oxide (ZnO) and aluminum nitride (AIN), which are piezoelectric materials that are widely used in PMUTs [14]. When an alternating electric field is applied between the top and bottom electrodes, stress is created in the in-plane direction of the piezoelectric layers, resulting in out-of-plane deflection of the membrane [12,14]. The vibration of the membrane generates acoustic sound waves that are transmitted into the surrounding medium. When the transmitted waves reflect back after hitting the medium, the membrane of the PMUT will be deflected. This deflection causes stress in the piezoelectric layers and consequently, an electric charge that can be detected and analyzed. Similar to CMUTs, the thin membrane increases the acoustic impedance matching with the surrounding medium and hence, eliminates the need

for acoustic matching layers. In contrast to CMUTs, the deflection of the membrane in PMUTs is not limited by the vacuum gap and for this reason, PMUTs can produce a higher acoustic output. Compared to bulk PZT transducers, the resonant frequency of the PMUT does not fully rely on the thickness of the piezoelectric layer, but as in CMUTs, it depends more on the dimensions, intrinsic stress and mechanical stiffness of the membrane [15]. The piezoelectrical signals generated in PMUTs require low voltage electronics compared to CMUTs, since PMUTs do not require high bias voltages and do not make use of external circuits to supply charge when signals are measured [12].

Important limitations of PMUTs are a low transmit sensitivity and a low coupling coefficient compared to bulk PZT ultrasound transducers and CMUTs [12]. Since the sensitivity is low, more input signal is required for acoustic output. Therefore, improving the sensitivity and coupling coefficient is taken into consideration during the design process of PMUTs. For instance, by optimizing material choice, electrode size and the thickness of the piezoelectric layers. Multiple studies have been conducted with the aim to increase the coupling coefficient of PMUTs. These studies include the development of piezoelectric materials with a high piezoelectric constant (Lead Magnesium Niobate/Lead Titanate, PMN-PT) [21], controlling residual stresses during the fabrication process (by depositing a SiO2 layer) [22], and optimizing the device structure, including partially clamped membranes [23], multi-electrode PMUTs [24] and 3D curved PMUTs [25].

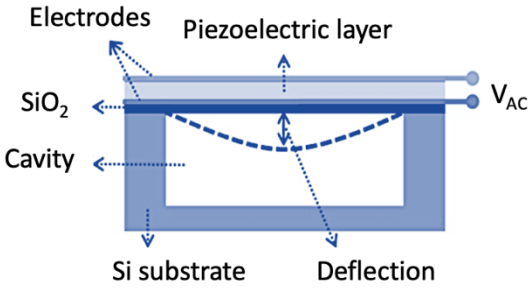

Figure 3 – Schematic view of a piezoelectric micromachined ultrasonic transducer (PMUT) consisting of a piezoelectric layer, electrodes and a passive layer (adapted from Ref. [15]).

2.2. *In vitro* neuromodulation

2.2.1. Conventional *in vitro* neuromodulation methods

Various researchers investigated low-intensity ultrasound stimulation of *in vitro* cell cultures, because the mechanical effects are known to modulate neurons and to promote different cell functions, such as stem cell differentiation and proliferation. Two configurations are used for ultrasound stimulation of *in vitro* cell cultures [26]. In one configuration, the petri dish and the ultrasound transducer are submerged in a deionized (DI) water tank, as shown in Figure 4a. The petri dish is located at the focal distance from the ultrasound transducer and the ultrasound waves are directed into the medium at an angle that enables imaging of calcium signals. The cells in the focal spot are primarily stimulated, which induces a calcium gradient. Subsequent waves induced by the calcium gradient propagate from the focal spot to adjacent regions, provoking calcium signaling responses from the cells in the surrounding regions. Therefore, cells in the focal spot are stimulated with a higher intensity than cells located at the surrounding regions [26,27]. For this reason, the configuration does not suit experiments that necessitate a

uniform and simultaneous stimulation. In the second configuration, the ultrasound transducer is located directly at the bottom of the petri dish, as shown in Figure 4b. The setup requires minimal acoustic coupling and decreases the chance of cell contamination [26]. However, the ultrasound waves are directed through the petri dish, which initiates distortion of the waves before stimulating the cells. This limits the setup in obtaining high acoustic output and uniform stimulation of the cells [26]. In addition, the second configuration is restricted to operate at low frequency (1 to 2 MHz) to compensate for the acoustic losses through the petri dish containing cells in culture [26]. The majority of previous *in vitro* neuromodulation studies are based on conventional bulk ultrasound transducers, which have disadvantages such as poor spatial resolution, non-uniform cell stimulation and high variability in experimental conditions due to lack of control over the acoustic parameters [28]. The development of microelectromechanical systems (MEMS) technology expanded the possibilities of *in vitro* neuromodulation methods and increased the spatial resolution. MEMS ultrasound transducers make localized and stable stimulation possible by using small transducers and by the capability of placing the cells on top of the transducers [28]. To overcome the aforementioned limitations, different studies developed piezoelectric micromachined LIFU transducers.

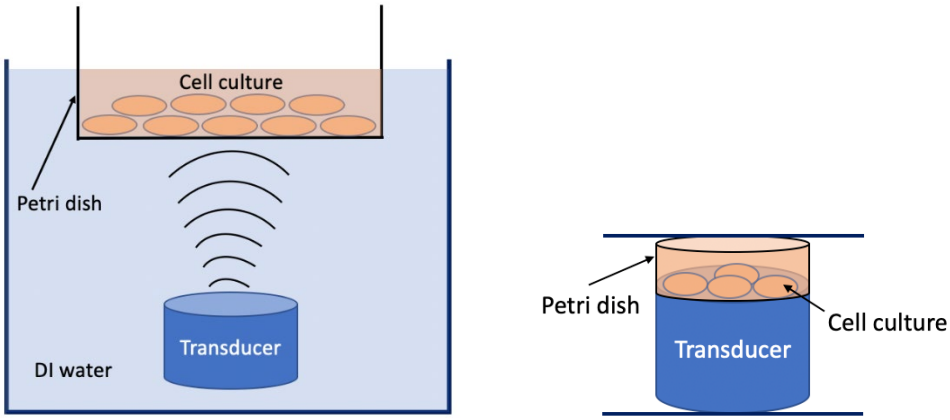

Figure 4 – Schematic view of the configurations used in in vitro studies for ultrasound neuromodulation: (a) immersion technique, (b) cell culture placed directly on transducer.

2.2.2. Ultrasound transducer characteristics for *in vitro* neuromodulation

J. Lee et al. fabricated a PMUT array composed of 16 transducer elements for modulating *in vitro* neuronal cells and brain slices with high spatial resolution [29]. The study found a resonant frequency of 430 kHz, which was shown to be a frequency that is suitable for modulating neurons. The acoustic intensity at the resonant frequency was measured with different input voltages to find the range of generated acoustic output. When the input voltage of the transducers varied from 11 to 66 V, the range of temporal peak acoustic intensity was 0.025 to 1.122 W/cm^2, which is high enough to modulate the neurons without causing thermal damage of the cells. An input voltage of 66 V corresponded to the highest response rate. Results have shown that the number of responding cells was proportional to the acoustic intensity. Furthermore, the transducer membrane was less than a millimeter (550 µm), making localized stimulation possible with high spatial resolution. The spatial resolution depends on the frequency. The higher the frequency, the smaller the transducer thickness and the higher the spatial resolution. To assess the capability of localized stimulation, the acoustic intensity was measured at horizontal distances from the center of the transducer. The study showed that the greater the horizontal distance from the center of the transducer, the smaller the acoustic intensity. The PMUT array has several advantages compared with conventional cell stimulating

methods, including high spatial resolution, accurate control of acoustic intensity and compatibility with *in vitro* cell cultures [29]. Choi et al. employed a focused ultrasound transducer with a center frequency of 500 kHz to modulate *in vitro* hippocampal neurons of rats and recorded the electric activities of the hippocampal neurons using a multielectrode array (MEA) [30]. The largest neuronal activity of the hippocampal neurons was measured at a pressure level of 0.8 MPa, with a spatial peak temporal average intensity (I_{spta}) of 16.14 mW/cm^2. The stimulation effects were also observed after exposure, indicating that ultrasound stimulation can modulate neuronal cells to be in an activated state for a short time after stimulation. Similar to the findings of the aforementioned study, Tyler et al. found that ultrasound with a frequency of 440 kHz, an I_{spta} of 23 mW/cm^2 and a pressure level of <1 MPa stimulates electrical activity in *in vitro* neurons by activating voltage-gated sodium and calcium channels [1]. Higher or lower intensities resulted in lower modulatory effects on neuronal cells. However, Kim et al. stimulated *in vitro* hippocampal slice cultures by applying an ultrasound frequency of 0.5 MHz and a spatial peak average intensity (I_{SPPA}) of 780 $\mu W/cm^2$, of which the latter is significantly smaller than the intensities used in previously reported studies. The ultrasound stimulation resulted in increased spike activity in the *in vitro* hippocampal slices during and after stimulation [31]. Another study applied high frequency ultrasound (7.75 MHz) to modulate the electrical excitability of *in vitro* hippocampal neurons [32]. Results of the study have shown that high frequency ultrasound increased the firing rates of neurons. From the findings of the discussed studies, it became evident that ultrasound has the potential to modulate neuronal cells. Nevertheless, the acoustic parameters, such as acoustic intensity, exposure time, acoustic frequency and pulse repetition frequency, should be taken into consideration to determine the effectiveness of modulating neurons. Further study of a range of stimulation parameters is required to understand the contributions of the waveform characteristics to the effects of ultrasound on neuronal activity.

2.3. Acoustic focusing

2.3.1. Acoustic lenses

Acoustic focusing is of importance for accurately stimulating *in vitro* cells with ultrasound. This can be achieved in different ways, as presented in Figure 5. Ultrasound can be focused using (1) a phased array that consists of multiple elements, each of which can be pulsed in a specific sequency with time delays in order to electronically steer the ultrasound beam in the desired direction. This method requires electrical connections and complicated phase regulation driving systems. Another method for acoustic focusing is by employing (2) a curved ultrasound transducer or attaching a convex or concave lens to a planar transducer. The lens concentrates the incident acoustic waves into the primary focus at the opposite side of the lens. Gradient cross-sectional acoustic lenses, which are similar to convex and concave optical lenses, converge or diverge the acoustic waves by creating a difference in propagation direction when the waves pass through the lens medium [33]. However, when the waves pass through the medium, scattering and internal absorption take place. This reduces the transmission efficiency. Furthermore, the challenge of the second method is the fabrication process where lens curvature errors and undesired surface roughness should be taken into account during manufacturing. When considering miniaturization of acoustic lenses, diffractive methods offer different advantages over traditional refractive methods. Traditional methods suffer from thicker profiles when curvature increases. Diffractive methods make use of flat and thin lenses, resulting in less internal absorption of energy. Furthermore, the lenses are compatible with

microfabrication technologies, increasing the design freedom [34]. Focusing ultrasound by the use of diffractive methods can be achieved through (3) Fresnel lenses, also known as Fresnel Zone Plates (FZPs). FZPs are an alternative for conventional curved acoustic lenses and are widely used because of less complex fabrication compared to conventional lenses. Fresnel lenses consist of a flat structure with multiple slits with decreasing width [33]. The sound waves pass through the slits and interfere with each other. Optimizing the selection of the geometric parameters of the slits allows for concentration of the acoustic waves at the primary focus with high precision. FZPs are used for many applications, such as ultrasound focusing applications. Acoustic FZPs often require the use of ultrasound emitters, of which the acoustic parameters can distort the energy distribution through the lens [35]. For that reason, it is important to incorporate emitter parameters, such as the frequency, in the design of the acoustic FZP.

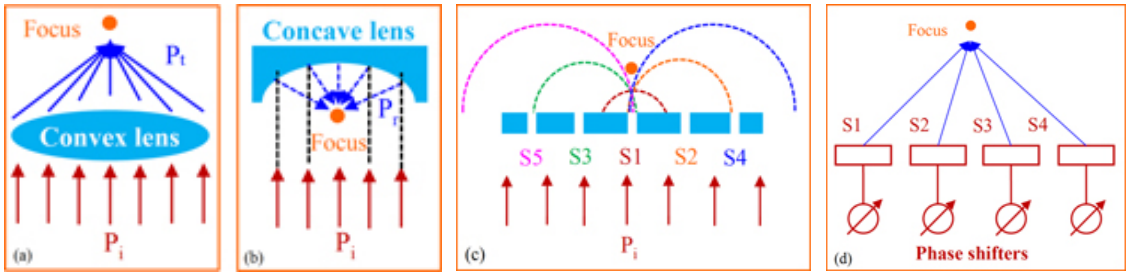

Figure 5 – Acoustic focusing methods: (a,b) gradient cross-sectional acoustic lenses, (c) acoustic Fresnel lens, (d) phased arrays. Reprinted from [33].

2.3.2. Fresnel lenses

FZP's can take on different forms. The traditional FZP consists of alternating absorbing blocking zones and transmitting transparent zones, as shown in Figure 6a. However, due to the absorbing zones the energy transmission efficiency is low (40% or less) [33]. The Fresnel Phase Zone Plate (FPZP), as presented in Figure 6b, introduces a phase shift of π by replacing the absorbing zones with thicker transparent zones, increasing the energy transmission efficiency. Figure 7 shows how the structure of the (multilevel) Fresnel lens approximates the spherical phase front of a concave lens. Acoustic FZP's that use multiple-phase levels in order to approach a spherical focusing field provide high energy transmission efficiencies [37]. The focusing efficiency is an important parameter that represents the ability of the lens to focus the energy in the desired direction and is defined as the percentage of the total incident energy at the lens that is found at the focus spot. Results of studies have shown that focusing efficiencies of 80% are achieved with multiple-phase levels Fresnel lenses, which is significantly higher compared to the efficiency of about 40% that is achieved with two-phase levels Fresnel lenses [38]. Chan et al. indicated a focusing efficiency of 81% for Fresnel lenses with multiple phase levels (4, 8 and 16 levels) by conducting finite element analysis (FEA) to predict the lens performance [39]. However, some significant aspects that could reduce the predicted total efficiency should be taken into consideration. Manufacturing errors or energy absorption in the lens and coupling medium can lead to a significantly lower transmission efficiency. A study evaluated the focusing efficiency of ultrasound energy for a fabricated Fresnel lens through FEA [37]. The focusing efficiencies of the designed and fabricated Fresnel lens were compared. It became evident that the focusing efficiency of the ideal four-phase levels Fresnel lens is approaching 75%, while the focusing efficiency of the fabricated four-phase levels Fresnel lens is approximate 63%. This difference is mostly caused by fabrication errors, such as over etching.

(a) (b)

Figure 6 – Fresnel zone plates: (a) traditional Fresnel Zone Plate, (b) Fresnel Phase Zone Plate.

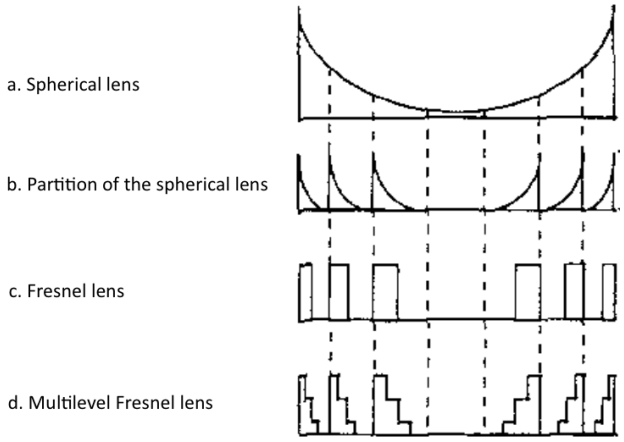

Figure 7 – Approximation of the spherical phase front by the (multilevel) Fresnel lens (adapted from Ref. [39]).

2.3.3. Design of acoustic Fresnel lens

An acoustic Fresnel lens can make use of multiple phase levels to mimic the phase curvature of a spherical focusing field in order to achieve high transmission efficiencies. Each ring on a Fresnel lens represents a zone, *k*. Increasing the number of Fresnel zones will increase the focusing gain [40]. However, increasing the number of Fresnel zones, will result in smaller zone pitches, making the fabrication process less reliable. The design of the multiphase levels Fresnel lens, as shown in Figure 8, is based on estimating the radial distances (r_k) and the step heights (h) that correspond to a given focal length and wavelength.

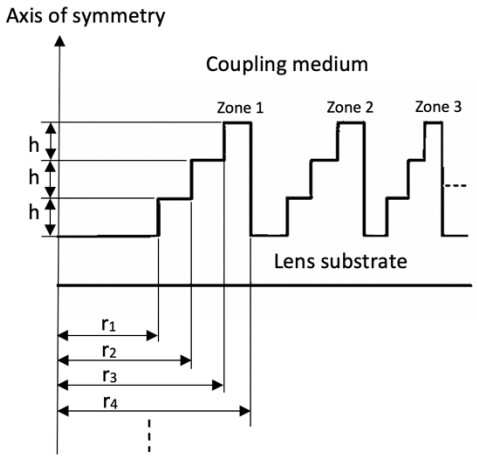

Figure 8 – Structure of a four-level Fresnel lens design; h is the step height and the r_k (k = 1,2,3…) is the radial distance (adapted from Ref. [41]).

The radial distance, r_k, is described by Equation (1), where z is the focal length of the lens, N is the number of phase levels, and λ is the wavelength of the acoustic field that is propagating through the coupling medium.

(1)
$$r_k = \left[\left(z + k\frac{\lambda}{N}\right)^2 - z^2\right]^{\frac{1}{2}}$$

The step height (h) between two-phase levels is given by Equation (2),

(2)
$$h = \frac{1}{Nf\left(\frac{1}{v_{cm}} - \frac{1}{v_{ls}}\right)}$$

where f is the frequency of the ultrasound produced by the transducer, v_{cm} is the speed velocity in the coupling medium and v_{ls} is the speed velocity in the lens substrate. According to the equations, a higher frequency results in smaller radials distances and step heights between phase levels. It is found that a maximum radial distance of 244 µm and a step height of 4.55 µm is required to operate at a frequency of 100 MHZ, while a 200-MHZ focusing lens requires a maximum radial distance of 122 µm and a step height of 2.27 µm [41]. The diffraction efficiency of an N-level lens, which is used to define the theoretically ideal value of the transmission efficiency, is described by Equation (3).

(3)
$$\eta = \left[\frac{\sin\left(\frac{\pi}{N}\right)}{\frac{\pi}{N}}\right]^2$$

2.3.4. Material selection and fabrication

Acoustic lens focusing requires variation in the speed of sound between different media. Hence, for selecting appropriate materials to be used as acoustic lenses, the speed of sound and the acoustic impedance of materials should be considered. The acoustic impedance, Z, describes the resistance to the propagation of acoustic waves within a medium and is given by Equation (4), where ρ is the material density (kg/m^3) and c is the speed of sound (m/s) in the material.

(4)
$$Z = \rho \mathrm{c}$$

If the acoustic impedances of two materials are similar, the amount of reflection will be minimized and therefore, more acoustic waves will be transmitted. When the acoustic impedances of two materials (Z_1 and Z_2) are known, the reflection and transmission coefficients at the interface of the two materials can be calculated. For normal incidence, the reflection coefficient, R, and transmission coefficient, T, are described by Equations (5) and (6), respectively.

(5)
$$R = \left[\frac{Z_2 - Z_1}{Z_2 + Z_1}\right]^2$$

(6)
$$T = \frac{4\,Z_1 Z_2}{(Z_2 + Z_1)^2}$$

In order to focus acoustic waves, it is important that the acoustic velocities in the medium and the lens material are different. The difference in acoustic velocities of the medium and the lens results in different refractive indices between the materials, leading to refraction of the

ultrasound beam [42]. However, achieving high transmittance of the acoustic waves requires the acoustic impedance of the lens material to be matched to that of the medium to decrease the amount of acoustic reflection and attenuation [43]. The configurations in the majority of *in vitro* neuromodulation studies are immersed in water, since water mimics soft tissue due to similar acoustic impedances. Therefore, in *in vitro* neuromodulation studies it is desired that the lens material is biocompatible and that the acoustic impedance of the lens material is close to that of water. Polymers are often used in MEMS technology due to rapid prototyping, easy fabrication and cost-effectiveness [44]. Polymethacrylate (PMMA), parylene and polydimethylsiloxane (PDMS) are polymers that are commonly used in acoustic lens applications due to their transparent properties [45,46,47]. The material properties of PMMA, parylene and PDMS are listed in Table 1.

Comparing the acoustic velocities of PDMS and water, a difference of approximately 40% is found. When comparing the acoustic velocities of PMMA and parylene with that of water, a significantly larger difference between the acoustic velocities is found. This difference between acoustic velocities is desired for achieving acoustic refraction for the focusing of the acoustic beam. However, the acoustic impedances of PMMA and parylene show a mismatch with that of water. This will result in poor transmission of the acoustic beam. On the other hand, PDMS has a similar acoustic impedance as water, which makes PDMS an useful material to be used in underwater configurations. Furthermore, PDMS has much higher elasticity compared to PMMA and parylene, which can be beneficial during fabrication processes or for focal length shifting by stretching the polymer [52]. Different studies employed PDMS as material for acoustic lenses used for piezoelectric ultrasound transducers [53,54,55]. In addition, PDMS offers advantageous features such as biocompatibility, low surface energy, thermal stability (up to 200°C), optical transparency and high stretchability [41,50,52]. Furthermore, PDMS is hydrophobic and able to adhere reversibly or, after oxidation, irreversibly to different types of substrates [54]. In terms of using PDMS as material in *in vitro* neuromodulation studies, it is found that PDMS can be used as a substrate in neurochips for the attachment and growth of neural cells, and differentiation of neural progenitor cells [56]. These attractive properties make PDMS a suitable material to be used in molding processes and as acoustic lens material in ultrasound applications for the stimulation of *in vitro* cells.

Medium	Speed of sound (m/s)	Density (kg/m^3)	Acoustic impedance (MRayls)	Young's Modulus (MPA)
PMMA [45,46]	2757	1180	3.25	3100 – 3300
Parylene [44,46]	2142	1289	2.76	4500
PDMS [41,47,48]	1077	969	1.04	1 – 3
Water [47]	1482	1000	1.48	-

Table 1 – Material properties of PMMA, Parylene, PDMS and water.

A two-phase levels Fresnel lens structure can be fabricated by exposing and developing negative photoresist on top of the silicon wafer. The patterned photoresist on the silicon wafer is used as a mold for PDMS, as shown in Figure 9. First, the negative photoresist is spin coated on the wafer. Then, the Fresnel lens structure is patterned on the silicon wafer. This is followed by pouring PDMS solution over the silicon-photoresist mold. The PDMS solution consists of a monomer and a curing agent, which are usually mixed at the ratio of 10:1 [44]. The PDMS solution is solidified at room temperature for 48h [57] or by baking the PDMS layer for 1 hour at 90 °C. Next, the PDMS is peeled off from the silicon-photoresist mold. An important limitation of this method is the maximum thickness of the photoresist that can be spin coated on the wafer, which depends on the type of photoresist that is used. Furthermore, it is difficult to have controlled thickness variation across a wafer with spin coating. Multiphase levels Fresnel lens structures require additional masking and etching steps. For 2^n phase levels, n masking steps are required [38]. For example, two masks are needed to make a four-phase levels Fresnel lens structure. A silicon mold is used for the fabrication of the multiphase levels Fresnel lens. The first mask with the design of the inverse Fresnel lens structure is used to make a two-phase levels Fresnel lens pattern, as shown in Figure 10. After exposure, the silicon mold is etched with the depth of 2h (h = step height of Fresnel lens). Thereafter, the mold is aligned and exposed using the second mask to transform the two-phase levels structure into a four-phase levels structure [37]. After exposure, the mold is etched with the depth of h. Then, PDMS is poured over the silicon-photoresist mold, solidified and separated, as in the fabrication of a two-phase level Fresnel lens structure. In both methods, the adhesion between the photoresist and PDMS and the adhesion between silicon and PDMS should be taken into consideration before peeling the PDMS layer off the mold.

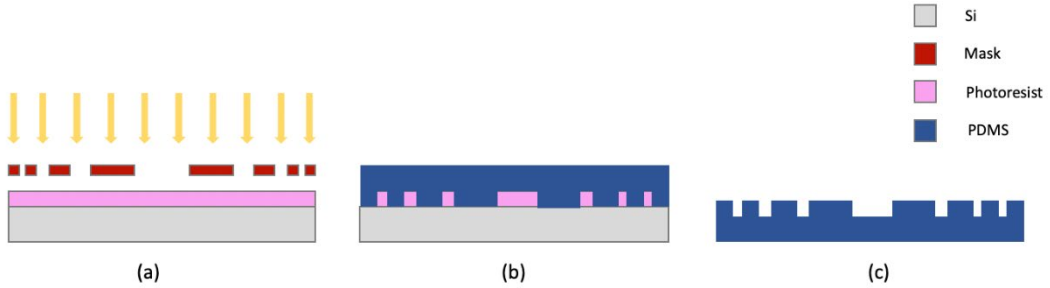

Figure 9 – Fabrication steps of two-phase levels Fresnel lens structure: (a) pattern the negative Fresnel lens structure on the silicon wafer, (b) pour the liquid PDMS on the silicon-photoresist mold and solidify, (c) peel off the PDMS layer.

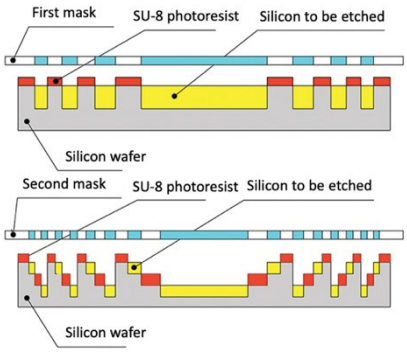

Figure 10 – Fabrication of a four-level Fresnel lens structure by using two masks (adapted from Ref. [37]).

2.4. Literature study - Discussion

2.4.1. Types of ultrasound transducers

In the literature study, different types of ultrasound transducers are discussed; the bulk piezoelectric ultrasound transducer and the micromachined ultrasound transducers (MUTs). The bulk ultrasound transducer is based on piezoelectric ceramics, such as PZT, and operates in the thickness direction when an alternating current is applied. The operating frequency depends on the piezoelectric layer thickness. The main drawbacks of the bulk ultrasound transducer are the large size dimensions, poor resolution and a high acoustic mismatch with the surrounding medium. Therefore, an acoustic matching layer, which improves the energy transmission efficiency, is often required to compensate for the high acoustic mismatch. The bulk piezoelectric ultrasound transducers are characterized by a high mechanical quality factor (Q), since bulk PZT transducers produce a spectrum with a high amplitude and a narrow range of operating frequencies. Consequently, the axial resolution is low, making bulk PZT transducers less suitable for ultrasound imaging applications. As for transmitting applications, the high Q in bulk PZT transducers provide high energy efficiency in the transmission of acoustic waves, reducing the electric input necessary for driving the PZT [58]. Furthermore, the high transmitting electroacoustic sensitivity of bulk PZT transducers leads to high pressures at the focal spot [59,60]. In comparison with bulk PZT transducers, micromachined ultrasound transducers (MUTs) have better acoustic impedance matching, operate at a larger frequency bandwidth and are compatible with CMOS processes.

The working principle of MUTs is either piezoelectric (pMUTs) or capacitive (cMUTs), both making use of thin films that function as flexible membranes. In contrast to bulk PZT transducers, MUTs provide high acoustic matching with soft tissue and can achieve small dimensions, making MUTs more appropriate to be used in small devices. In pMUTs, an alternating electric field is applied between the top and bottom electrodes, resulting in vibration of the flexible membrane, often made of PZT, ZnO or AlN. Important limitations of pMUTs are the low transmitting electroacoustic sensitivity and coupling coefficient. As a consequence, pMUTS are more suited for applications in the low-frequency range, such as sensing applications [15]. Although both pMUTs and cMUTs operate with flexural membranes, there are several differences between the transducers. A cMUT element is driven by electrostatic force due to changes in capacitance, while pMUTs are based on piezoelectricity. Furthermore, cMUTs make use of high biasing voltages. The transmit sensitivity of cMUTs is higher when compared to pMUTs, but still lower than that of bulk PZT transducers [59,60]. In addition, the Q of cMUTs is much lower in comparison with PZT. In contrast to bulk PZT transducers and pMUTs, the low Q of cMUTs results in a wider bandwidth and hence, better axial resolution. Therefore, cMUTs are more suited to operate in the high frequency range and for imaging applications.

For the purpose of *in vitro* neuromodulation, cMUTs are not often used because they require complex fabrication and operate in the high frequency range. *In vitro* neuromodulation studies frequently employ pMUTs, since pMUTs operate in the low frequency range. Furthermore, pMUTs provide localized uniform stimulation of *in vitro* cells, whereas in bulk PZT transducers the cells are non-uniformly stimulated, resulting in different outcomes between experiments. Consequently, consistency of the acoustic stimulation parameters, such as duration and pulse repetition frequency, is difficult to attain between repetitive experiments. However, the high Q and transmitting electroacoustic sensitivity of bulk PZT transducers are desirable to achieve high power efficiency and high intensities at the focal spot. In addition, the

low transmit sensitivity of pMUTs require higher input voltages, which are located close to the cells. Consequently, this can negatively influence the ultrasound stimulation of the cells. The transmit sensitivity of bulk PZT can even be more increased when a matching layer with high acoustic impedance and small acoustic attenuation is used [61]. In addition, the development of piezoelectric materials with a high piezoelectric coefficient, such as PMN-PT, will increase the coupling coefficient and transmit sensitivity [21].

2.4.2. Ultrasound transducer characteristics and *in vitro* neuromodulation

Different studies investigated the ultrasound transducer characteristics for *in vitro* neuromodulation, yet only a small part of the studies reports *in vitro* results where the ultrasound and stimulation parameters are highly controlled and the applied pressure is specified. Several researchers developed micromachined LIFU transducers because of the many advantages it provides over conventional *in vitro* neuromodulation methods, including increased spatial resolution, improved control of stimulation parameters and biocompatibility. However, the micromachined LIFU transducers are still prone to errors. One issue to address is wave reflection. This is not only the case with conventional configurations in which the transducer and the cell culture plate are immersed in water, but also with configurations in which the transducer is placed directly below a cell culture plate and where the cell culture is exposed to air. The wave reflection is attributed to a difference in acoustic impedances and affects the reliability of the stimulation conditions.

Another important problem to resolve is understanding the effects caused by the acoustic waveform characteristics on neuromodulation. From the results of the discussed studies, it can be concluded that there is no clear relationship between the driving voltage and the output acoustic pressure in the different studies, because each transducer can have different efficiencies and topologies. Characterization of stimulation is solely based on acoustic properties. Furthermore, it is found that cell stimulation effects depend on both the frequency and energy density, of which the last is the product of the acoustic intensity and exposure time [62]. *In vitro* ultrasound neuromodulation studies typically employ transducers with a frequency range of 100 kHz – 10 MHz [5,27,29,30,32]. The choice of frequency depends on the type of study. *In vitro* studies with the purpose of determining if a LIPU therapeutic treatment is completely safe, controllable and repeatable, focus on frequencies that are suitable for transcranial ultrasound stimulation where the frequency is limited due to skull attenuation. Studies that are focused on *in vitro* purposes only, can utilize a wider frequency range, going up to 1 GHz [63]. The acoustic parameters, such as exposure time, pulse repetition frequency and acoustic intensity, will most likely determine the effectiveness of the acoustic waves on modulating neuronal activity. Further research of the interactions between different acoustic parameters is required to understand the influence of ultrasound on neuronal activity.

2.4.3. Acoustic Fresnel lens

In order to stimulate *in vitro* cells with ultrasound, the ultrasound beam needs to be focused at the target. In this literature study, different ways to achieve acoustic focusing are described. A phased array bulk ultrasound transducer electronically steers the ultrasound waves to create constructive interference of the waves, resulting in the ultrasound beam to be focused at the desired angle. The setup relies on many external electronics for the regulation of the different phases and driving the transducer. However, these electronics can be implemented on a complementary metal oxide semiconductor (CMOS) for phased arrays, but this requires complex and expensive fabrication [60]. A single element transducer focuses the ultrasound

beam by either using a curved piezoelectric transducer or adding a lens on top of a planar transducer. Convex and concave lenses are based on refractive properties and are sensitive to scattering and internal absorption when waves pass through the lens medium, which results in reduced transmission efficiency. Furthermore, convex or concave lenses are sensitive to fabrication errors, including shape and curvature errors and undesired surface roughness. Fresnel lenses are based on diffractive properties and make use of flat and thin lenses, resulting in less internal absorption of energy and thus, increased transmission efficiency. Furthermore, the lenses are compatible with microfabrication technologies and are less sensitive to fabrication errors compared to curved acoustic lenses. Various studies showed that multiple-phase levels Fresnel lenses achieve significantly higher focusing efficiencies compared to a Fresnel lens that consists of two-phase levels [38,39,40]. This can be explained by the fact that multiple-phase levels Fresnel lenses achieve a closer approach to the spherical focusing field than two-phase levels Fresnel lenses do and therefore, multiple-phase levels Fresnel lenses increase the transmission coefficient. A high transmission coefficient will subsequently result in an increased focusing gain. Moreover, adding more Fresnel zones in the design of the Fresnel lens will also contribute to improving the focusing gain and higher spatial resolution.

The geometry of the acoustic Fresnel lens is based on the transducer parameters, such as frequency and wavelength. Increasing the frequency, results in acquiring more zones by decreasing the radial distances and step heights between phase levels. From this it can be hypothesized that using an acoustic Fresnel lens on top of a transducer with a high frequency will result in a higher focusing gain compared to a transducer with a lower frequency. However, the reliability of the fabrication process should be taken into account when increasing the number of Fresnel zones in the design of the lens, since the width of the rings become smaller with each zone. Very small feature sizes, e.g. <50 µm, are more prone to manufacturing errors, which consequently could affect the performance of the lens.

2.4.3.1. Acoustic lens materials

The material of the acoustic lens should meet two important requirements. Firstly, the acoustic velocity of the lens material should differ with that of the medium in order to increase diffraction and focusing effects. Secondly, the acoustic impedance of the lens material should be similar to that of the medium to increase the transmission of acoustic waves. In this literature study, water is chosen as medium, since it represents soft tissue. From the comparison between material properties of different polymers, it became clear that the acoustic and mechanical properties of PDMS meet the requirements for the material choice of the acoustic lens. Other advantages of PDMS include biocompatibility, transparency, thermal stability, low surface energy and high elasticity. The low surface energy and high elasticity of PDMS facilitates the release from molds. Furthermore, the mechanical properties of PDMS can be altered when the monomer and mixing agent are mixed at different ratio [50]. The high hydrophobicity of PDMS can form a limitation in some applications, for example, when cell cultures are placed on top of PDMS for cell attachment and growth [56]. In these cases, hydrophilic modification of PDMS, such as oxygen plasma treatment, is required [44,64].

2.4.3.2. Acoustic lens fabrication

The fabrication process of two types of PDMS molds are discussed in the literature study; the photoresist mold and the silicon mold. The photoresist mold presents some limitations. Since the step height of PDMS must be equal to the thickness of the photoresist layer, the maximum thickness of photoresist that can be spin coated may result in challenges regarding the design.

In addition, controlled thickness variation across the wafer is difficult to achieve, which is required in the case of multiple-phase levels Fresnel lenses. A silicon mold encounters less difficulties, because the mold can be etched to obtain the desired step heights of the Fresnel lens. Due to the strong adhesion between the silicon mold and PDMS, coating the mold with an anti-adhesive layer is required for peeling off the PDMS without damaging the mold or the PDMS structure. Polytetrafluoroethylene (PFTE), also referred to as Teflon, is well-known for its anti-adhesive properties, resistance to molecular adsorption and chemical inertness [65]. Therefore, Teflon is a suitable candidate to be used as anti-adhesive layer between the silicon mold and PDMS.

2.5. Literature study – Conclusion and Recommendations

The presented literature study gained information from previous studies to provide insight into the question: How to design and fabricate an acoustic lens to place on the surface of an ultrasound transducer for focusing acoustic waves to stimulate *in vitro* neuronal cells? The goal of the present study is to focus the ultrasound waves at the location where the cell culture is placed by using an acoustic lens. In this study, uniform stimulation of the cells and consistency of the stimulation parameters is of less importance. The main focus of the research is achieving the desired focal length, a small focal spot size and high intensities at the focal spot in order to assess the performance of the acoustic lens. From the findings it became clear that among the types of ultrasound transducers, the bulk piezoelectric transducer is most appropriate for achieving high power efficiency and high intensities at the focal spot due to its high Q and high transmitting electroacoustic sensitivity. The transmit sensitivity of the bulk PZT transducer can even be further improved by using piezoelectric materials with a high piezoelectric constant or by using a matching layer with an acoustic impedance between that of PZT and water.

Fresnel lenses provide attractive properties for the design of the acoustic lens. Compared to other types of lenses, Fresnel lenses are compatible with microfabrication technologies and the fabrication is less complex. From the literature study, it became evident that the use of multi-phase levels Fresnel lenses achieves high transmission efficiencies compared to a two-phase levels Fresnel lens. Furthermore, the design of the Fresnel lens is based on the frequency of the ultrasound transducer. The higher the frequency, the higher the number of Fresnel zones due to smaller radial distances and thus, the higher the focusing gain. For this reason, using an acoustic Fresnel lens on top of an ultrasound transducer with a high frequency will result in an increased intensity at the focal spot and a higher spatial resolution of the focus spot.

The material choice for the acoustic Fresnel lens depends on several factors, such as optical transparency, acoustic velocity and acoustic impedance. A significant difference in acoustic velocity between water and the lens material is required, whereas the acoustic impedance of the lens material is required to be close to that of water. From comparing different polymers, it was found that the acoustic, optical and mechanical properties of PDMS make it a suitable material to be used as acoustic lens material in underwater configurations. With regard to the fabrication process, a silicon mold provides several advantages compared to a photoresist mold. A silicon mold facilitates the fabrication of multi-phase levels Fresnel lenses. The mechanical properties of PDMS, such as high elasticity, makes the release from molds easy. However, an anti-adhesive layer, such as Teflon, is required between the mold and the PDMS to prevent PDMS sticking to the mold.

2.6. Research plan

The goal of the research is to design and fabricate an acoustic lens, which can be placed on top of an ultrasound transducer, in order to focus the ultrasound waves at a pre-determined focal length (6.5 – 7 mm) to fit into the currently used MEA devices, as demonstrated in Figure 11. At this distance from the transducer, the cell culture with neuronal cells is located. Based on the findings of the literature study, bulk PZT transducers with a high frequency (12 MHz and 16 MHz) will be employed and the design of the acoustic lens will be based on Fresnel lenses.

First, calculations of the lens radii and step height are carried out for the design of a two-phase levels acoustic Fresnel lens. Next, simulations of the PDMS acoustic lens on top of the ultrasound transducer are performed in COMSOL Multiphysics® to assess the performance of the designed acoustic Fresnel lenses. The following properties of the designed acoustic Fresnel lens are examined for the 12 MHz and 16 MHz ultrasound transducer: Focal length, number of zones, smallest feature size of the lens and the focus spot size.

Subsequently, calculations for the design of a multiphase levels acoustic Fresnel lens and corresponding simulations in COMSOL Multiphysics are carried out. If the results acquired by the simulations of the two-phase levels and multiphase-levels acoustic Fresnel lenses are significant, the acoustic Fresnel lens is fabricated. The design of the acoustic Fresnel lenses will be converted into a photomask containing the lens structures. The photomask is required for the lithography steps in the fabrication process and is designed in the software Tanner L-edit (Layout Editor). For the fabrication of the acoustic Fresnel lens, a silicon wafer is chosen to be used as a mold. The silicon mold is patterned using the photomask.

The ultrasound transducer exists of a bottom chip, which is connected to electronics for driving the PZT, and a cap on which the acoustic Fresnel lens is placed. The integration of the bottom chip, cap and acoustic Fresnel lens will form the final product. After finalization of the fabrication process, the ultrasound transducer with acoustic lens is tested in an underwater configuration using a hydrophone. The focal length, acoustic intensities at the focal spot and the focal spot size are measured.

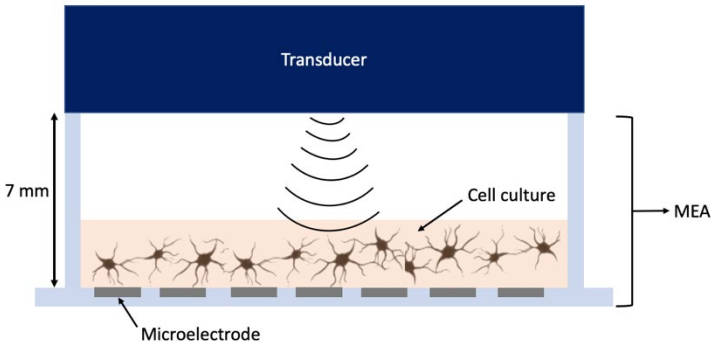

Figure 11 – Concept image of the ultrasound neuromodulation system using the transducer and the MEA device.

3. Methods

This chapter presents the design, the simulations acquired with COMSOL Multiphysics® and the microfabrication of the acoustic Fresnel lens. Furthermore, it describes the microfabrication of the cap and the assembly process of the ultrasound transducer. For the microfabrication of the acoustic Fresnel lens and the cap, the machinery in the clean rooms of Else Kooi Laboratory (EKL) at TU Delft are utilized. After explaining the microfabrication and the post-processing steps of the required elements for the final product, the experimental measurement set-up is described.

3.1. Design acoustic Fresnel lens

The design of the two-phase levels acoustic Fresnel lens, as shown in Figure 12, includes calculations of the radial distances (r_k) and step height (h) corresponding to the focal length and wavelength. The wavelength is equal to the wavelength of the acoustic field through the PDMS medium, which is the ratio between the speed of sound through PDMS (c_{pdms} = 1077 m/s) and the transducer frequency. The calculations are based on Equations (1) and (2), defined in Chapter 2.3.3. For the two-phase levels acoustic Fresnel lens, the value of N is 2. The focal length in Equation (1) is set at 9 mm instead of the pre-determined focal length of 7 mm, in order to compensate for the concept of focal shift, which is often seen in devices with small Fresnel numbers [63]. The concept of focal shift implies that the focal length shifts backwards towards the lens and consequently, results in a smaller focal length [60,66]. Another design parameter is the number of lens zones (k), which is related to the transducer diameter and frequency. Increasing the transducer diameter or the transducer frequency, results in an increase in the number of zones. Calculations of the lens radii and step heights are carried out for acoustic lenses designed for frequencies of 12 MHz and 16 MHz. The lens radii and step heights of the acoustic two-phase levels Fresnel lens are listed in Appendix A. The design parameters of the acoustic two-phase levels Fresnel lens are summarized in Table 2.

For the design of the multiphase levels acoustic Fresnel lens (Figure 8), the calculations of the lens radii and step heights are repeated, where the value of N is equal to 4. The focal length is again set at 9 mm. The design parameters of the multi-phase levels acoustic Fresnel lens are summarized in Table 3.

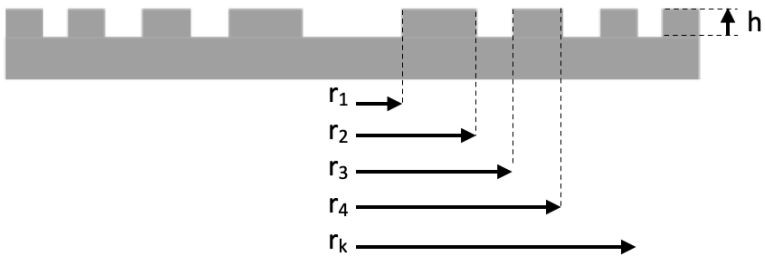

Figure 12 – Schematic cross section of the two-phase levels acoustic Fresnel lens.

	12 MHz	16 MHz
Inner radius (µm)	900	780
Outer radius = lens radius (µm)	2877	2950
h (µm)	164	123
Number of zones	10	14
Minimum feature size: $r_{k,max} - r_{k,max-1}$ (µm)	151	110

Table 2 - Design parameters of the two-phase levels acoustic Fresnel lens for transducer frequencies 12 and 16 MHz.

	12 MHz	16 MHz
Inner radius (µm)	636	551
Outer radius = lens radius (µm)	2950	2950
h (µm)	164	123
Number of zones	21	28
Minimum feature size: $r_{k,max} - r_{k,max-1}$ (µm)	73	54

Table 3 - Design parameters of the four-phase levels acoustic Fresnel lens for transducer frequencies 12 and 16 MHz.

3.2. Simulations in COMSOL Multiphysics

A simplified cross-sectional model of an ultrasound transducer with a radius of 3 mm is shown in Figure 13a. The COMSOL Multiphysics simulation conditions are listed in Appendix B (Table B.1). The transducer consists of silicon parts, an air gap and a PZT element. Next, the acoustic two-phase levels lens with a radius of 3 mm, which is designed according to the used transducer frequency and pre-set focal length of 9 mm, is placed on top of the ultrasound transducer. Figure 13b presents the model including the PDMS acoustic Fresnel lens. Simulations are conducted for the 12 MHz and 16 MHz ultrasound transducers to evaluate the performance of the designed acoustic Fresnel lens. Figure 14 compares the two-dimensional acoustic intensities parallel to the transducer with and without an acoustic lens on top of the transducer. As shown in Figure 14, when no acoustic lens is employed, the acoustic waves are dispersed in the medium without focusing at one point. The simulations have shown that the acoustic Fresnel lens focuses the ultrasound beam. The acoustic waves are focused at a focal length of 6.6 mm for transducer frequency 12 MHz and at a focal length of 6.7 mm for transducer frequency 16 MHz, which is within the desired range of the pre-determined focal length. Furthermore, when the substrate thickness of the acoustic Fresnel lens is varied, no significant changes are seen in the results, as demonstrated in Figure 15. The acoustic waves are still focused at the same focal length. For this reason, the substrate thickness of the acoustic Fresnel lens is of less importance and the efficiency of the lens is mainly based on the radial distances and the step height.

To determine the focus spot size, the full width at half maximum (FWHM) is measured. The width of the focus spot is equal to the FWHM acquired by the acoustic intensity perpendicular to the transducer, as shown in Figure 16(a,b). The acoustic intensity perpendicular to the transducer is measured at 6.6 mm and 6.7 mm distance from the transducer, which are the focal lengths for the 12 MHz transducer and the 16 MHz transducer, respectively. From Figure 16(c,d), it can be seen that the focus spot is centered with small size and high intensity when a two-phase levels acoustic lens is employed. The length of the focus spot is equal to the FWHM of the peak of focus derived from the acoustic intensity profile parallel to the transducer.

The focus spot characteristics are summarized in Table 4. It can be seen that the focus spot size is smaller for higher frequencies, which is desired for the stimulation of neuronal cells.

Subsequently, the multiphase levels acoustic lens with a radius of 3 mm is placed on top of the ultrasound transducer in the model, as shown in Figure 17. Simulations are carried out for transducer frequencies 12 MHz and 16 MHz. The acoustic intensity, parallel to the transducer, is plotted in Figure 18. The acoustic waves are focused at a focal length of 6.3 mm for transducer frequency 12 MHz and at a focal length of 6.6 mm for transducer frequency 16 MHz. Comparing the acoustic intensities of the models with the two-phase and multiphase levels acoustic lenses, the intensities at the focus spot are significantly smaller when using a multiphase levels acoustic lens. This is in contrast to the findings of the literature study. Hence, it became apparent that the design of the multiphase levels acoustic lens is not yet optimized.

From the outcomes of the COMSOL simulations, using models with acoustic lenses on top of ultrasound transducers with frequencies 12 MHz and 16 MHz, it can be seen that the multi-phase levels acoustic Fresnel lens behaves less reliable compared to the two-phase levels acoustic Fresnel lens. The two-phase levels acoustic Fresnel lens has the most promising results by achieving high intensities at the focus spot within the range of the desired focal length, i.e. 6.5 – 7 mm. Furthermore, the ultrasound transducer frequency of 16 MHz produces a smaller focus spot size compared to the transducer frequency of 12 MHz. Based on these findings, the fabrication process will focus on the two-phase levels acoustic Fresnel lens and the emphasis will be on the 16 MHz ultrasound transducer. However, transducer frequency 12 MHz will be verified as well. In addition, acoustic lenses with dimensional sizes of 8x8 and 10x10 mm will be examined to assess whether a greater number of zones in the acoustic lens, while preserving the frequency, will result in an improved focusing gain. The radial distances used for the design of the 6x6, 8x8 and 10x10 mm two-phase levels acoustic Fresnel lenses and the 3x3 multiphase levels acoustic Fresnel lenses are listed in Appendix A. Simulations performed for the 10x10 mm acoustic Fresnel lens are presented in Appendix B (Figure B.1, Figure B.2).

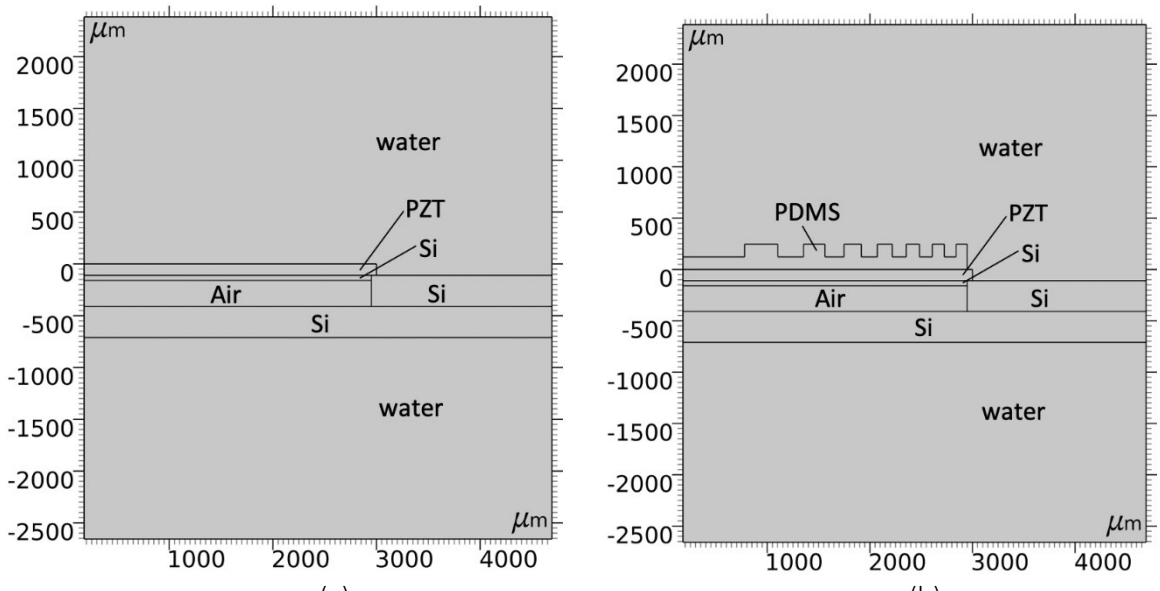

Figure 13 – COMSOL models: (a) model of the ultrasound transducer with r = 3 mm, (b) model of a PDMS two-phase levels acoustic Fresnel lens placed on top of the ultrasound transducer.

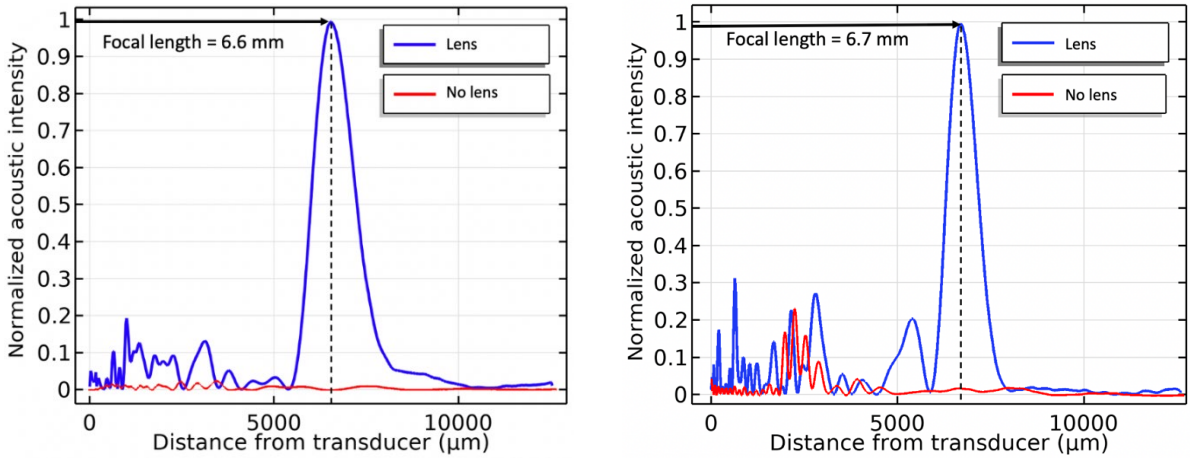

(a) (b)

Figure 14 – Acoustic intensity, parallel to the transducer, with and without a two-phase levels acoustic lens on top of the transducer. The focal length is 6.6 mm for transducer frequency 12 MHz (a) and 6.7 mm for transducer frequency 16 MHz (b).

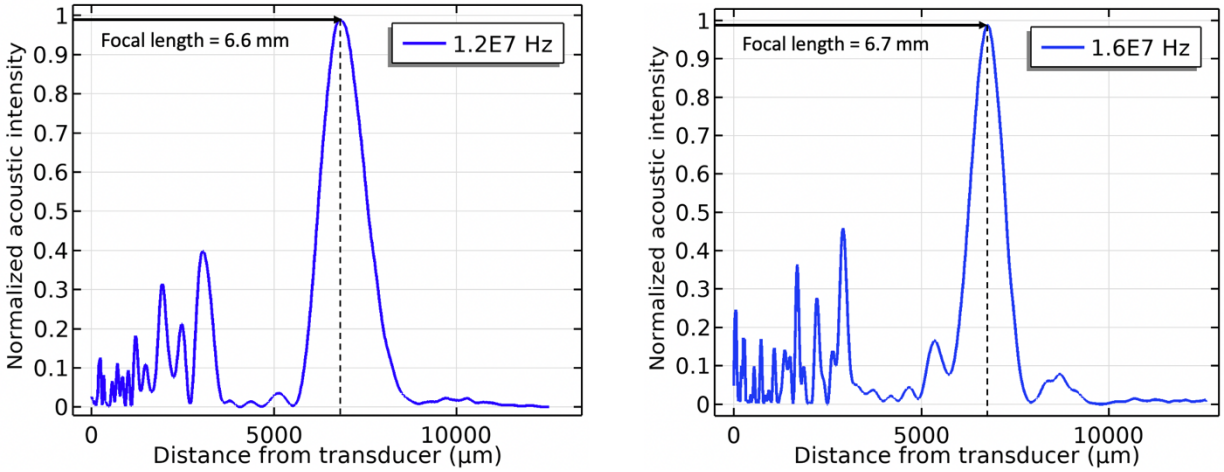

(a) (b)

Figure 15 – Acoustic intensity, parallel to the transducer, using a two-phase levels acoustic lens with increased lens substrate thickness (+200µm) on top of the ultrasound transducer. The focal length is 6.6 mm for transducer frequency 12 MHz (a) and 6.7 mm for transducer frequency 16 MHz (b).

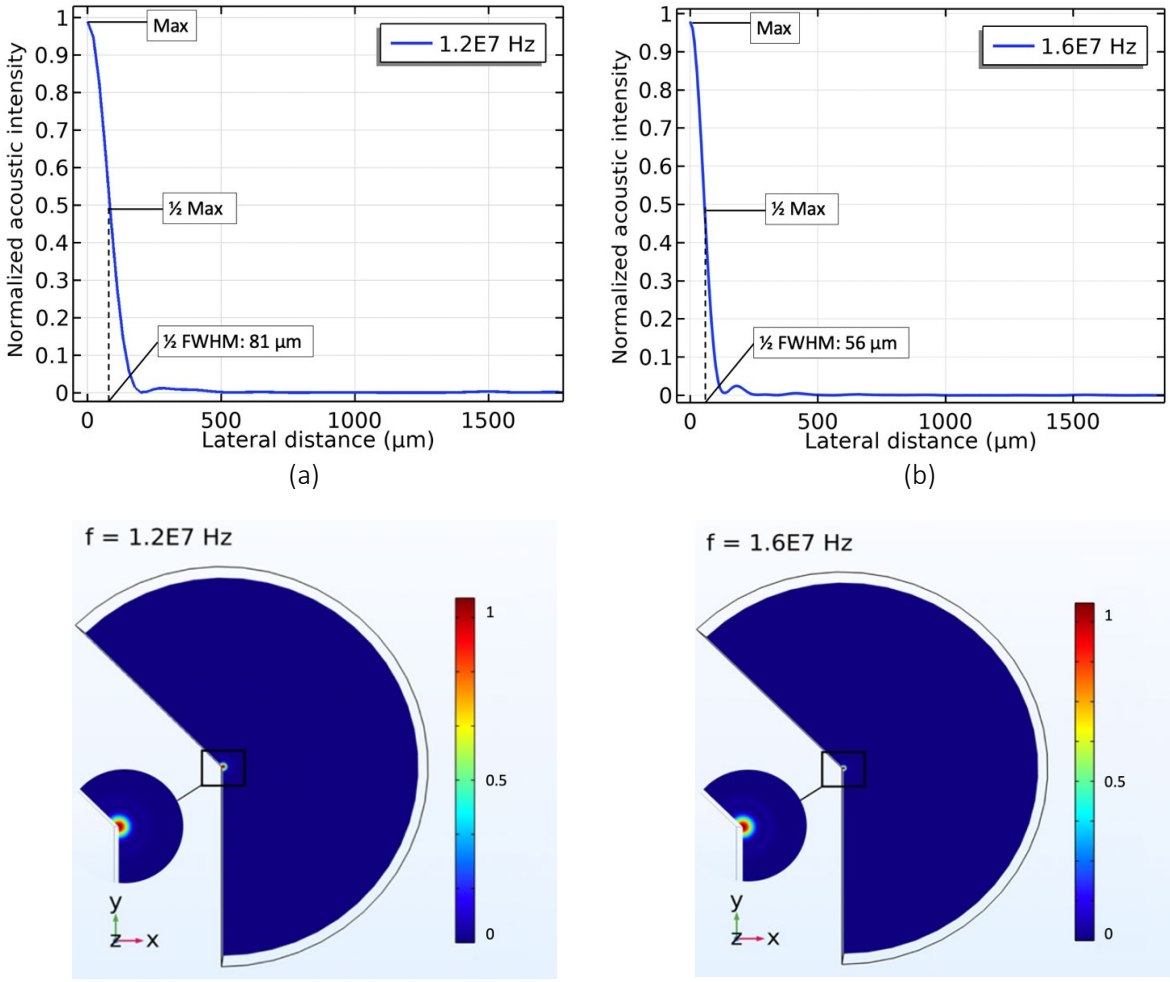

Figure 16 – Two-dimensional (a,b) and three-dimensional (c,d) acoustic intensities perpendicular to the transducer using a two-phase levels acoustic lens on top of the 12 MHz ultrasound transducer (a,c) and the 16 MHz ultrasound transducer (b,d).

	12 MHz	16 MHz
Focal length (mm)	6.6	6.7
Width of focus spot (µm)	162	112
Length of focus spot (µm)	1210	919

Table 4 – Characteristics of the focus spot derived from COMSOL simulations of using two-phase levels acoustic Fresnel lenses on ultrasound transducers (12 MHz, 16 MHz).

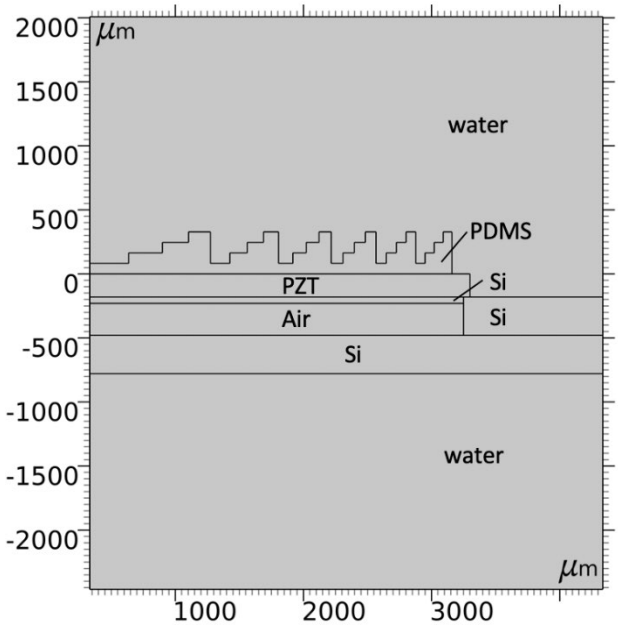

Figure 17 – COMSOL model of a PDMS multi-phase levels acoustic Fresnel lens on top of an ultrasound transducer.

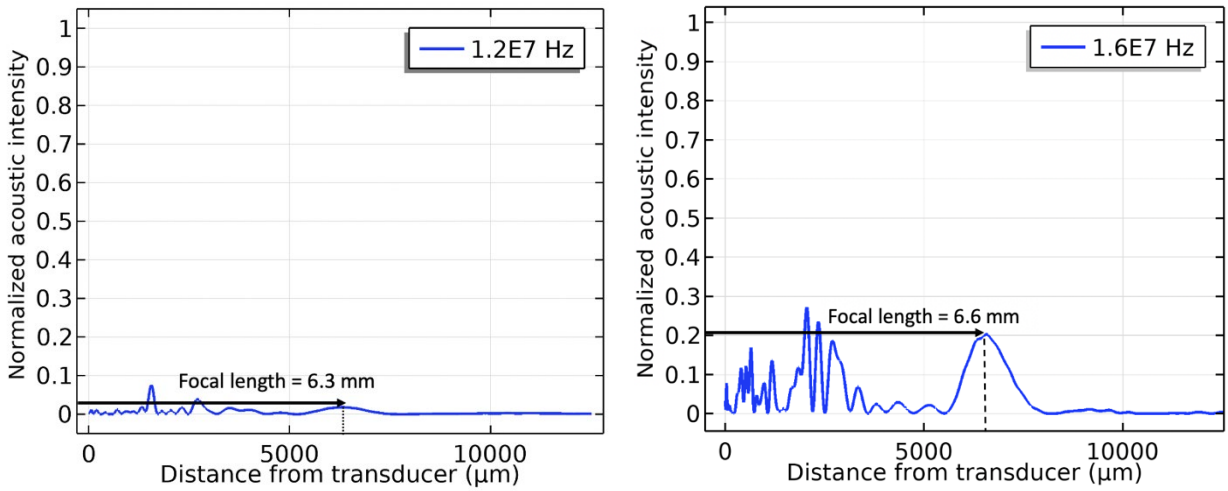

Figure 18 – Acoustic intensity, parallel to the transducer, using a multi-phase levels acoustic Fresnel lens on top of the transducer. The focal length is 6.3 mm for transducer frequency 12 MHz (a) and 6.6 mm for transducer frequency 16 MHz (b).

3.3. Microfabrication acoustic Fresnel lens

An overview of the fabrication of the acoustic two phase-levels Fresnel lens is shown in Figure 19, which consists of the fabrication of a silicon mold through standard photolithography methodologies and deep reactive ion etching (DRIE). A detailed description of the fabrication process of the acoustic Fresnel lens can be found in the flowchart presented in Appendix C. The fabrication process starts with a 500 μm single side polished (SSP) wafer. An oxide layer of 500 nm is deposited through Plasma Enhanced Chemical Vapor Deposition (PECVD). Next, the wafer is spin coated with negative photoresist (2000, AZ® nLOF) at 1060 revolutions per minute (rpm) for 30 seconds to achieve a photoresist thickness of 3.5 μm. Before the start of the fabrication process, a photomask is designed in the software Tanner L-edit. The photomask is required for the exposure step in the fabrication process. Printing the features in darkfield or bright field polarities should be considered during the design. The choice of polarity depends on the to be used photoresist and whether subtractive or additive processes are used during fabrication for achieving the desired pattern. The design of the two-phase levels acoustic Fresnel lens is converted into a photomask in which more space is allocated for the acoustic Fresnel lens designed for the 16 MHz transducer, as shown in Figure 20. For the fabrication of the silicon mold, negative photoresist is used. Therefore, a bright field chromium (Cr) photomask is employed. Figure 21 shows the final photomask.

After exposure and development, the developed negative photoresist layer acts as a masking layer for etching the silicon dioxide (SiO_2), as shown in step 4 of Figure 19. The etch rate of PECVD oxide and buffered hydrofluoric acid (BHF) (1:7) is 250-300 nm/min. To remove 500 nm of oxide, a total etch time of 2 minutes, and 30 seconds of over-etching is maintained. The remaining photoresist layer is removed in an oxygen plasma, using the Tepla plasma system. In step 5 of the fabrication process, the oxide layer acts as a masking layer for DRIE to obtain the desired structures for the silicon mold. An etching depth of 123 μm is required for the design of the acoustic Fresnel lens using a transducer frequency of 16 MHz, as listed in Table 2. The remaining oxide layer is etched for 2 minutes and 30 seconds with BHF (1:7), similar to step 4 of Figure 19.

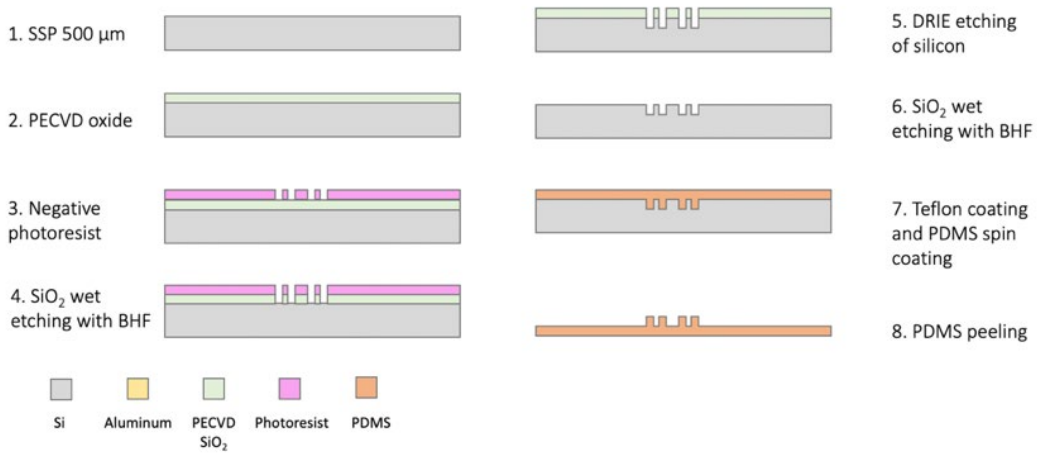

Figure 19 – Diagram of the fabrication process of acoustic two-level phase Fresnel lens: (1) on a 500 μm single side polished (SSP) wafer, (2) deposit oxide layer through PECVD, (3) patterning with negative photoresist NLOF, (4) etch SiO_2 to create masking layer, (5) create silicon mold through DRIE, (6) etch remaining SiO_2, (7) coat silicon mold with Teflon and spin coat PDMS on the silicon mold, (8) peel PDMS off.

The silicon mold is then coated with Teflon. This is followed by spin coating PDMS (Sylgard 184, Dow Corning) on the silicon mold. The Sylgard 184 PDMS kit consists of a silicone elastomer base and a curing agent. The two components are mixed with a ratio 10 (elastomer) to 1 (curing agent). The liquid PDMS is spin coated on the silicon mold. The final thickness of the PDMS layer depends on the spin coating speed (rpm) and the spinning time. To achieve a PDMS thickness of 163 μm, the spin coating speed is set at 600 rpm for 20 seconds. The silicon mold with the spin coated liquid PDMS is placed inside a vacuum chamber for degassing. Next, the PDMS is cured at 90 °C for 1 hour. After baking, the PDMS is manually peeled off from the mold, as demonstrated in Figure 22a. Figure 22b shows the individual lenses, which are manually cut out from the PDMS layer with a blade.

The features of the fabricated PDMS acoustic lenses are examined using a microscope (VK-X250, Keyence). The profiles of the two extremes, i.e. the 6x6 mm and the 10x10 mm acoustic Fresnel lenses, are presented in Figure 23. From Figure 23, it can be observed that the radial distances between the zones decreases as the number of zones increases. The different radii of the 6x6 mm and the 10x10 mm fabricated acoustic Fresnel lenses are presented in Figure 24 and Figure 25, respectively. The features of the designed acoustic Fresnel lenses are compared to the features of the fabricated acoustic Fresnel lenses. From Table 5, it can be observed that similar results are seen between the features of the designed and fabricated 6x6 mm acoustic Fresnel lens with a maximum error of 1.3%. Table 6 shows the comparison between the designed and fabricated 10x10 mm acoustic Fresnel lens. A maximum error of 10.2% is found for the smallest feature of the lens. Small features, i.e. <70 μm, are more sensitive to fabrication errors and require more wet etching time to allow the etchant to reach the surface under the opening of the masking layer. Therefore, the mismatch between the designed and fabricated features is mostly caused by the occurrence of under-etching during step 4 of the fabrication process (Figure 19).

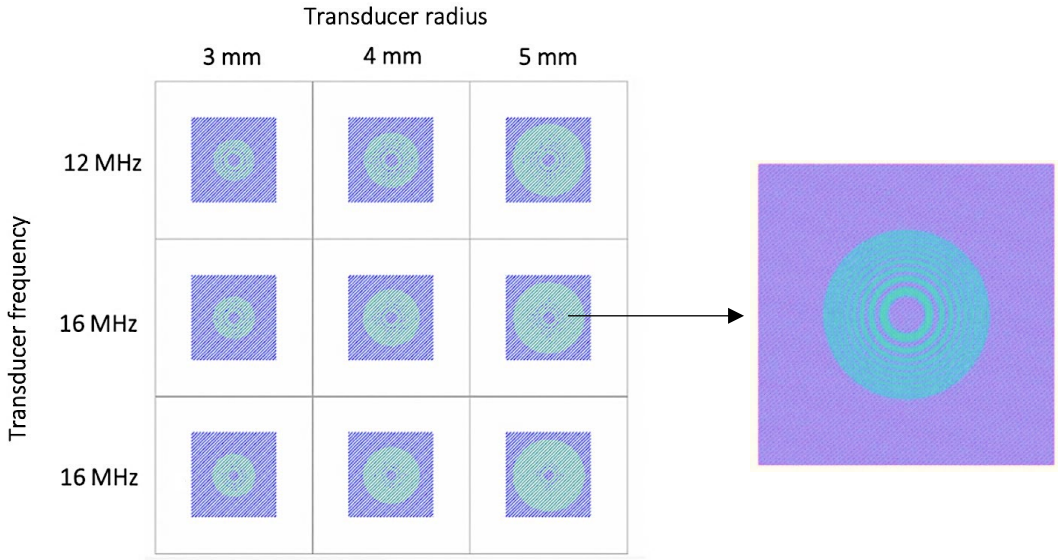

Figure 20 – Bright field photomask containing the two-phase levels acoustic Fresnel lens design (green = Cr, blue = transparent opening of 12 x 12 mm).

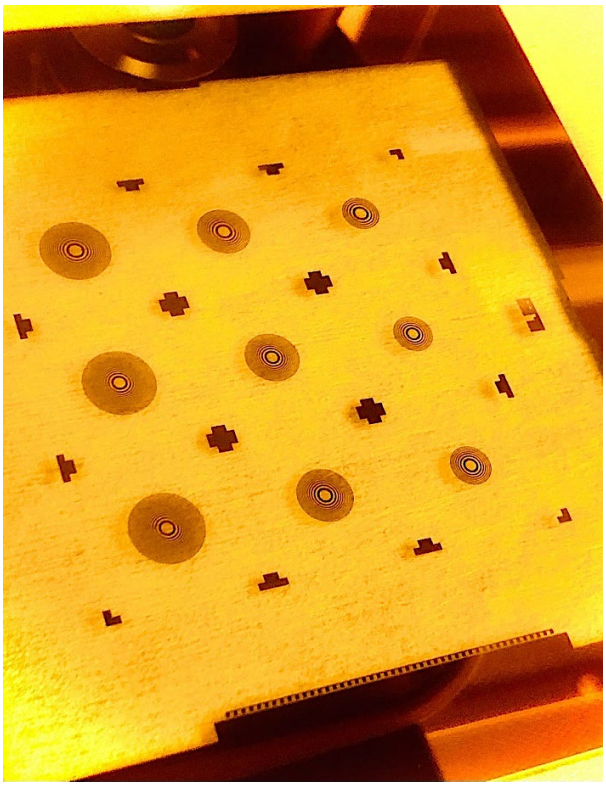

Figure 21 – Optical image of the chromium photomask containing the two-phase levels acoustic Fresnel lens structures for the silicon mold.

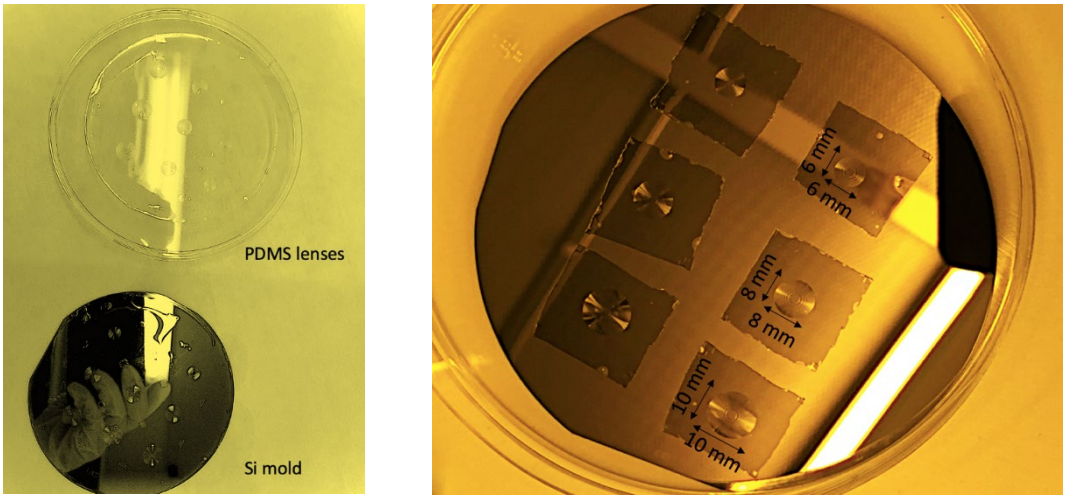

(a) (b)

Figure 22 – Optical image of acoustic Fresnel lenses: (a) acoustic Fresnel lenses peeled off from the silicon mold, (b) individual acoustic Fresnel lenses cut out from the PDMS layer.

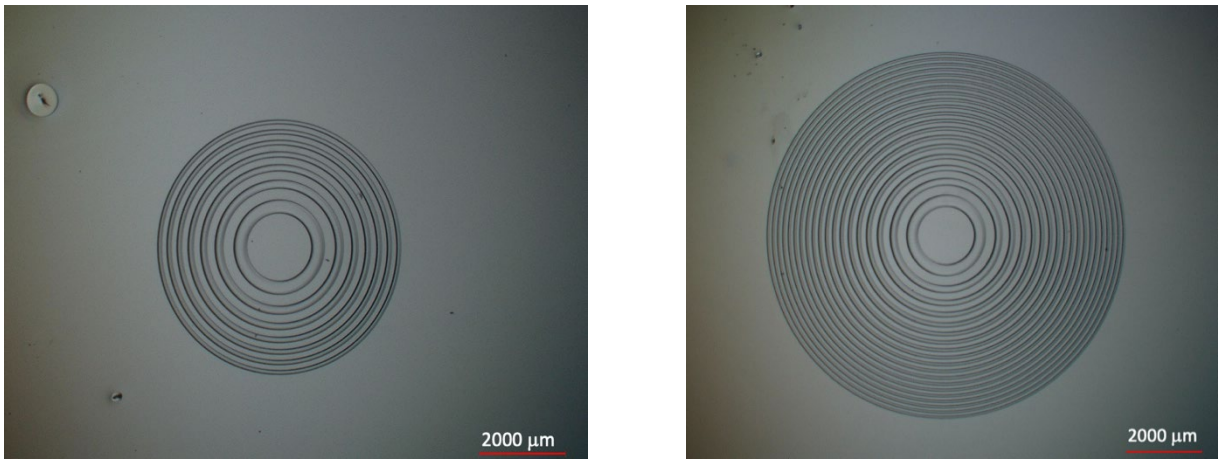

(a) (b)

Figure 23 – Optical profiles of the fabricated acoustic Fresnel lenses acquired with microscopy: (a) 6x6 mm acoustic Fresnel lens, (b) 10x10 mm acoustic Fresnel lens.

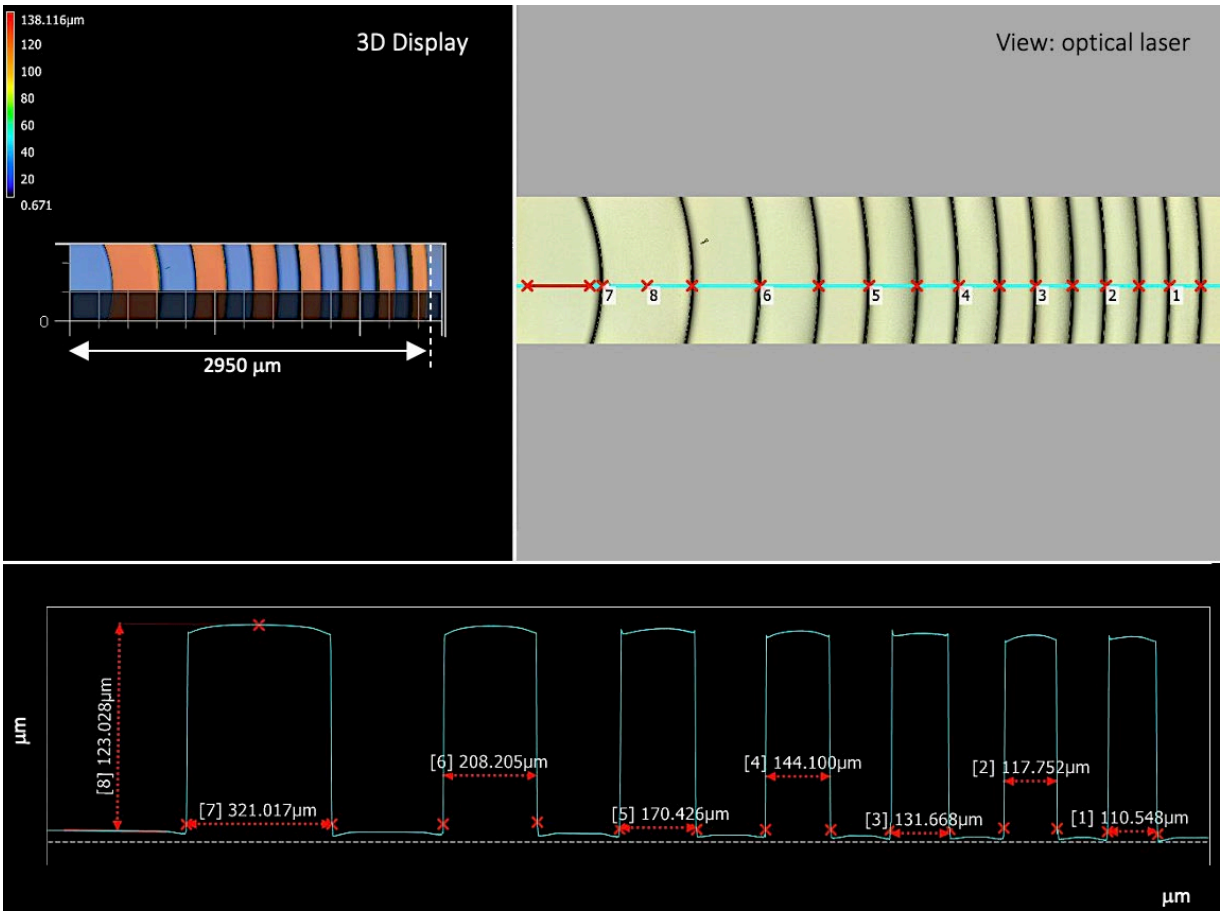

Figure 24 – Optical profiling of the step height and radii (µm) of the fabricated 6x6mm two-phase levels acoustic Fresnel lens.

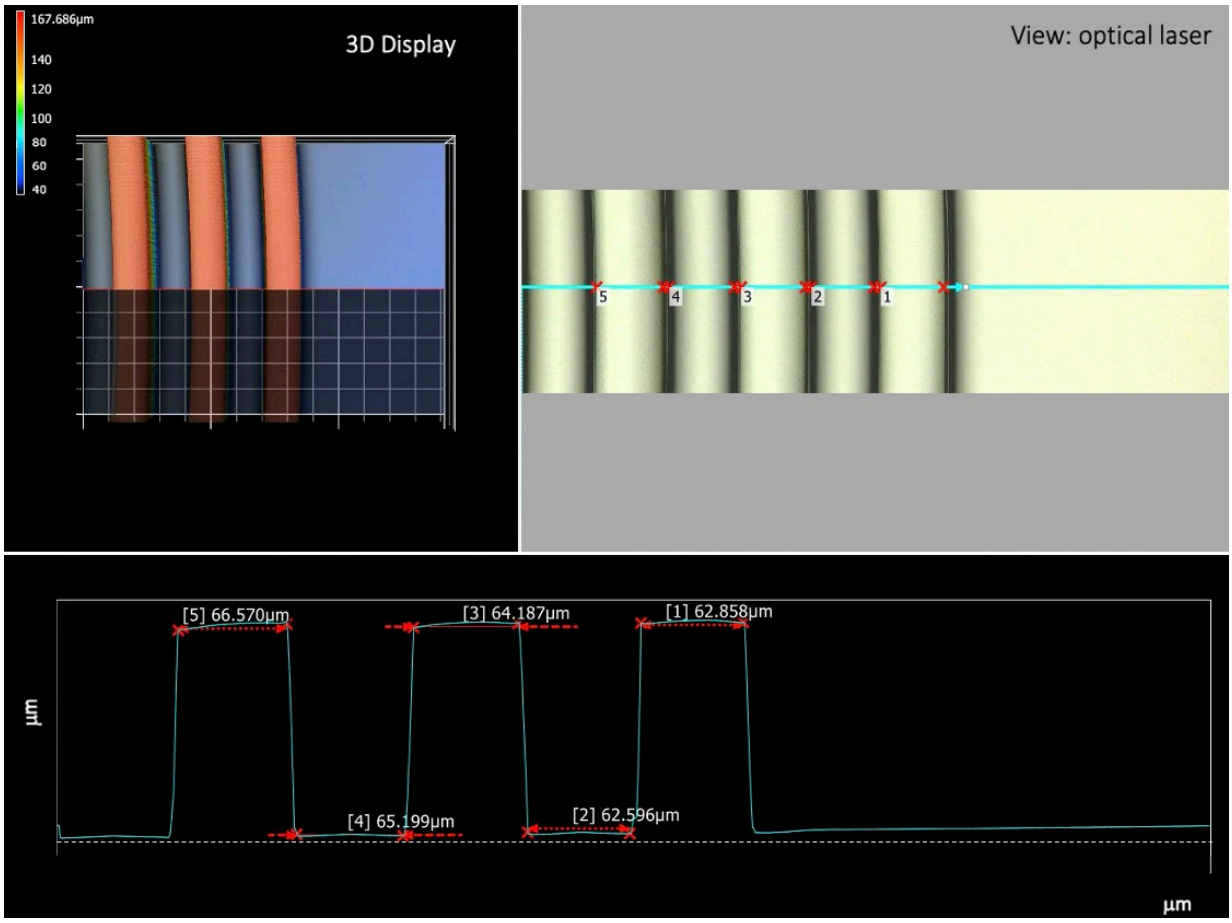

Figure 25 – Optical profiling of the radii (µm) of the fabricated 10x10 mm two-phase levels acoustic Fresnel lens. The outer three radii are shown.

r_k (µm)	Radii design (µm)	Radii fabricated lens (µm)	Error (%)
r_7 (outer ring, smallest resolution)	110	110.55	0.5
r_6	118	117.75	0.2
r_5	130	131.67	1.3
r_4	145	144.10	0.6
r_3	169	170.43	0.8
r_2	211	208.21	1.3
r_1 (inner ring)	324	321.02	0.9

Table 5 – Comparison between the designed 6x6 mm acoustic Fresnel lens and the fabricated acoustic Fresnel lens.

r_k (µm)	Radii design (µm)	Radii fabricated lens (µm)	Error (%)
r_{19} (outer ring, smallest resolution)	70	62.86	10.2
r_{18}	71	64.19	9.6
r_{17}	73	66.57	8.8

Table 6 – Comparison between the designed 10x10 mm acoustic Fresnel lens and the fabricated acoustic Fresnel lens. The outer three radii are listed.

3.4. Microfabrication cap

For driving the transducer, an electrical field has to be generated on top and bottom of the PZT. However, the implementation of a top-level connection using microfabrication techniques is difficult due to the PZT thickness. For instance, typical techniques used in microfabrication, such as sputtering or evaporation, deposit thin films in the nanometer scale, whereas the PZT thickness is in the micron scale. To overcome this challenge, a microfabricated conductive membrane on silicon is introduced, also referred to as the cap. The cap consists of a thin aluminum layer, providing a top-level connection to the PZT and closing the electric circuit. Furthermore, the cap provides a surface on which the acoustic Fresnel lens can be placed. PDMS is chosen to be used as support layer in the cap to minimize acoustic mismatching between the cap and the acoustic Fresnel lens. Furthermore, the acoustic Fresnel lens is made of PDMS and, as shown in the simulations (Figure 15), the thickness of the lens substrate doesn't influence the results. Therefore, PDMS is a good material to be used as support layer in the cap, since the acoustic Fresnel lens is placed directly on the PDMS side of the cap. The cap consists of three gaps, of which the outer two gaps are used for making interconnects to the bottom chip, as shown in Figure 26. The purpose of the middle gap is to create a membrane structure for the PZT to be placed underneath. The height of the gaps is equal to the PZT thickness, which depends on the frequency of the PZT.

The fabrication process of the cap is presented in Figure 27. First, the silicon wafer is thinned down using DRIE to match the PZT thickness of 150 μm. An oxide layer of 6 μm is deposited on the frontside of the wafer through PECVD. Next, an aluminum layer of 400 nm is sputtered on top of the oxide layer. To carry out step 5 of the fabrication process, a photomask is required for the lithography step. Since positive photoresist (AZ12XT-20PL) is used for the fabrication of the cap, a darkfield Cr photomask is utilized. A mask overview of the cap and the acoustic lens is illustrated in Figure 28. After patterning the backside of the wafer, the silicon was etched from the back using DRIE to create the membrane structure and the contact openings. This is followed by spin coating 100 μm-thick PDMS (Sylgard 184, Dow Corning) on the aluminum layer on the frontside. The spin coating speed is set at 900 rpm for 40 seconds to define the thickness. The PDMS layer is cured at 90 °C for 1 hour. Then, the silicon dioxide layer is removed by using BHF (1:7). An etch time of 25 min is required to fully remove the silicon dioxide layer. However, at approximately 14 minutes, BHF started etching the aluminum layer. This resulted in delamination of the PDMS layer at the edges of the wafer and for this reason, the etching process could not be continued. Finally, the wafer was diced. The cap structure is shown in Figure 29.

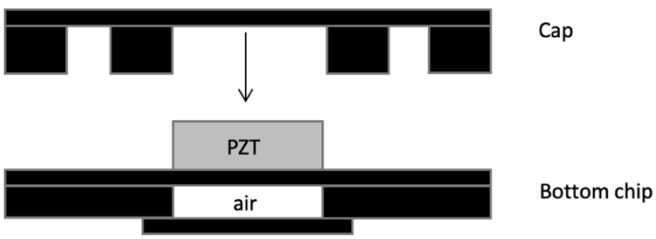

Figure 26 – Schematic view of the cap and bottom chip.

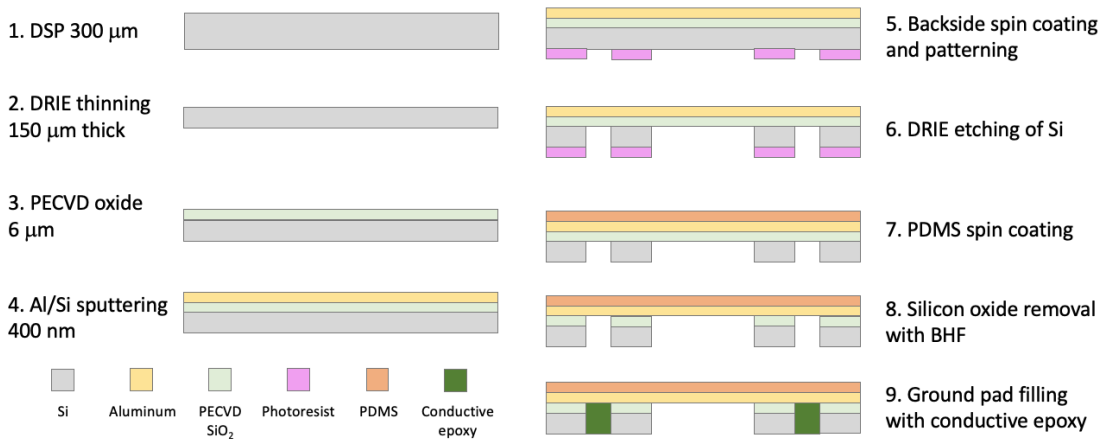

Figure 27 – Diagram of the fabrication process of the cap: (1) on a 300 µm double side polished (DSP) wafer, (2) thinning the wafer to match the PZT thickness, (3) deposit oxide layer through PECVD, (4) sputtering of Al(99%)/Si(1%), (5) backside spin coating with positive photoresist (AZ 12XT-20PL) and patterning, (6) backside DRIE to create the membrane and contact openings, (7) spin coating of PDMS on frontside, (8) etching of SiO_2 using BHF (1:7), (9) filling contact opening with conductive epoxy to create interconnects.

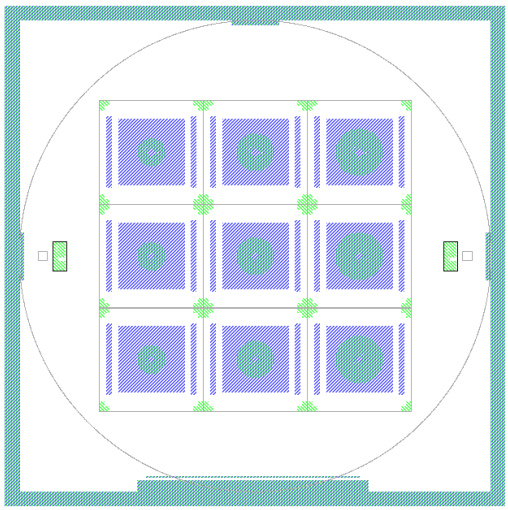

Figure 28 – Two-layer mask overview including the acoustic Fresnel lens and cap designs: (blue) darkfield mask for the backside opening of the cap, (green) bright field mask for the silicon mold.

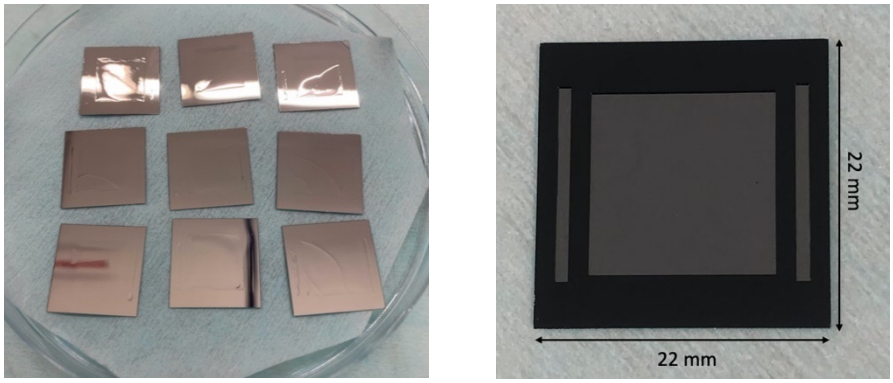

(a) (b)

Figure 29 – Optical images: (a) Top view of the diced caps, (b) bottom view of a single cap structure.

3.5. Integration process

3.5.1. Conductive interconnects

The contact openings of the cap were filled with silver epoxy (H20E, Epo-Tek) to create conductive interconnects, as shown in Figure 30a. The silver epoxy was cured at 90° C for 3 hours on a hotplate (Thermo Scientific SP88857107). After curing, the conductivity of the cap was measured within the conductive vias and across the cap using a multimeter (973A, Hewlett Packard). The measurements showed high resistance in the MΩ-range and hence, a bad conductivity. An important factor that may could reduce the conductivity, is the relatively large particle size (≤ 45 μm) of the silver particles in silver epoxy [67]. For this reason, conductive paste (42469, Alfa Aesar) is introduced to fill the contact openings of the cap. The conductive paste consists of smaller particles compared to that of silver epoxy, which is demonstrated in Figure 31. The contact openings of the cap were filled with conductive paste, as shown in Figure 30b, and then cured at 90° C for 15 minutes on the hotplate. Next, the conductivity was measured between different points in the cap (Figure 32a). The resistance within the contact vias was 1 Ω. The measurement showed significantly improved conductivity compared to filling the contact openings with silver epoxy. However, the resistance across the cap was still high, i.e. 1.8 MΩ. This can be explained by the remaining silicon dioxide in the cap openings, which was not fully removed because of the reduced etching time. Since inserting the wafer or individual caps in BHF (1:7) resulted in delamination of the PDMS layer, a new method is required for fully removing the silicon dioxide. In this new method, drops of BHF (1:7) are directly applied on the silicon dioxide areas at the backside of the cap and thus, avoiding the aluminum layer to be etched through the frontside of the cap. Next, the contact openings of the cap were filled with conductive paste and cured at 90° C for 15 minutes on the hotplate. After curing, the conductivity of the cap was measured. The resistance within the contact vias was measured at 0.6 Ω and the resistance across the cap at 20 Ω (Figure 32b). Therefore, using drops of BHF directly on the silicon dioxide areas of the cap showed significantly increased conductivity.

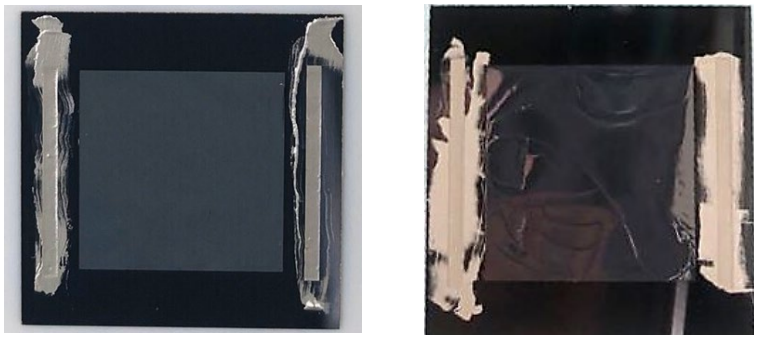

(a) (b)

Figure 30 – Optical images of the contact openings filled with:
(a) conductive silver epoxy (H20E, Epo-Tek), (b) conductive paste (42469, Alfa Aesar).

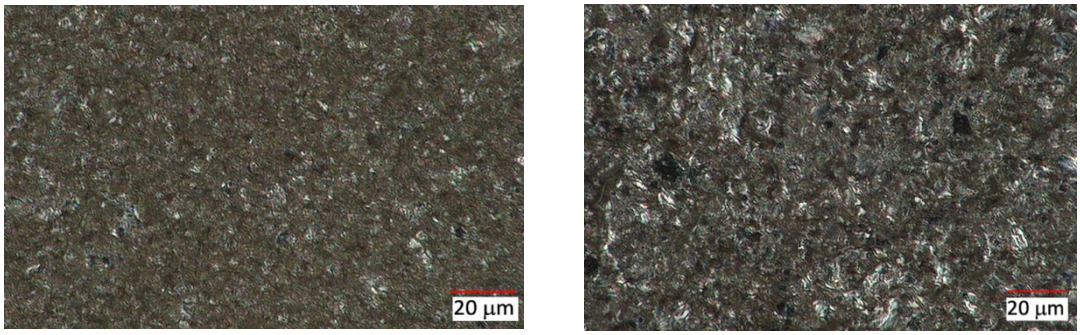

(a) (b)

Figure 31 – Magnified particle size: (a) conductive paste (42469, Alfa Aesar), (b) conductive silver epoxy (H20E, Epo-Tek).

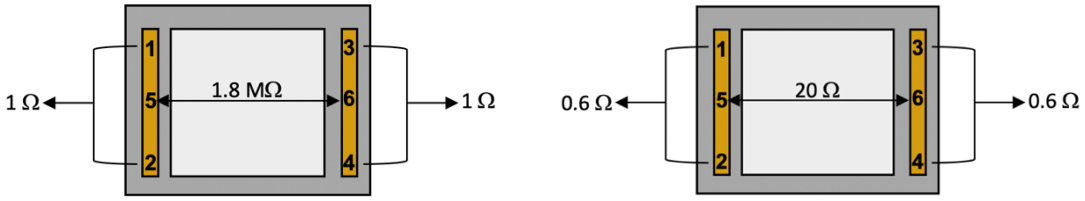

(a) (b)

Figure 32 – Resistance of the cap measured from point 1 to point 2, point 3 to point 4 and point 5 to point 6: (a) Placing the cap in a BHF (1:7) bath and filling the contact openings with conductive paste, (b) BHF (1:7) drops on silicon dioxide areas only and filling the contact openings with conductive paste.

3.5.2. Top and bottom level connection

The bottom-level connection is provided by a test chip. The test chip contains pads for bottom and top connections, a single bulk PZT element in the middle and four metal pins for driving the transducer, as demonstrated in Figure 33a. Furthermore, the backside of the test chip consists of an opening equal to the size of the PZT element, which is sealed by a glass plate using non-conductive epoxy (301-2FL, Gentec), as shown in Figure 33b. This creates an air gap to improve the efficiency of the transducer. Figure 34 presents the fully integrated chip, in which the cap is attached to the test chip using silver epoxy. This results in a top connection to the PZT and closing the electric circuit. The conductivity of the fabricated chip is measured at 17.7 Ω across the Al/PDMS membrane, as can be seen in Figure 35. From this, it became evident that the cap provides a top-level connection to the PZT by creating an electric field. Next, the top side of the chip was sealed with non-conductive epoxy to avoid contact with deionized (DI) water when testing the chip in an underwater configuration. However, after sealing with non-conductive epoxy, the conductivity of the chip was decreased significantly with a resistance measured in the MΩ-range.

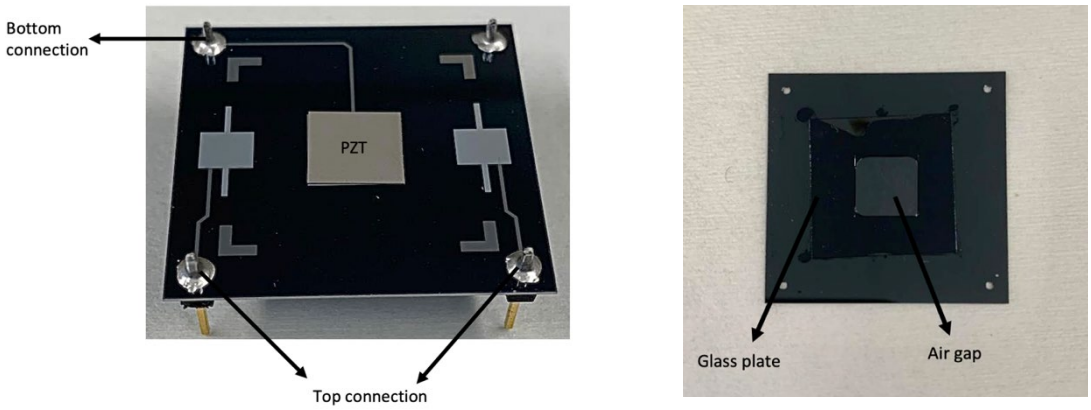

(a) (b)

Figure 33 – Optical images of the test chip: (a) top view of the test chip, (b) bottom view of the test chip.

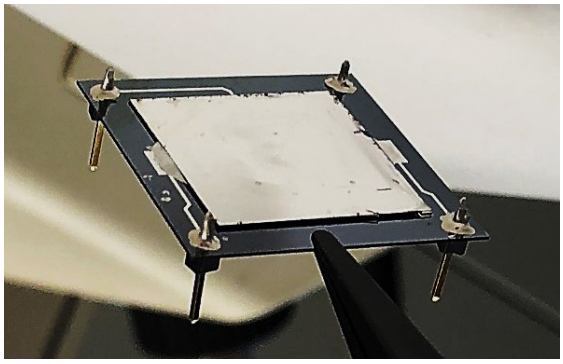

Figure 34 – Optical image of the cap structure attached on top of the test chip using silver epoxy (H20E, Epo-Tek).

Figure 35 – Optical image of the conductivity measured across the Al/PDMS membrane.

3.6. Test chip

For the purpose of the study, it was decided to continue with the test chip only considering the problems experienced with the cap. Figure 36a presents the test chip, where a single bulk PZT element (with a dimensional size of 6x6, 8x8 or 10x10 mm) is attached to the test chip using conductive paste. The conductive paste is cured at 90° C for 15 minutes on the hotplate. The metal pins are replaced by two tungsten wires (99.95%, 0.05mm, annealed), attached with conductive paste, to provide a closed electric circuit, as shown in Figure 36b. The surface of the PZT element is covered with conductive paste to ensure that the PZT can be driven across its entire surface. Again, the conductive paste is cured at 90° C for 15 minutes on the hotplate. Next, the test chip is sealed with parylene to avoid contact with DI water when testing the chip in an underwater configuration. Finally, the acoustic Fresnel lens with corresponding diameter was manually aligned and mounted on the test chip (Figure 36b). No adhesive was needed between the test chip and the acoustic lens, since the adhesion between the parylene layer of the test chip and the PDMS acoustic Fresnel lens was strong enough.

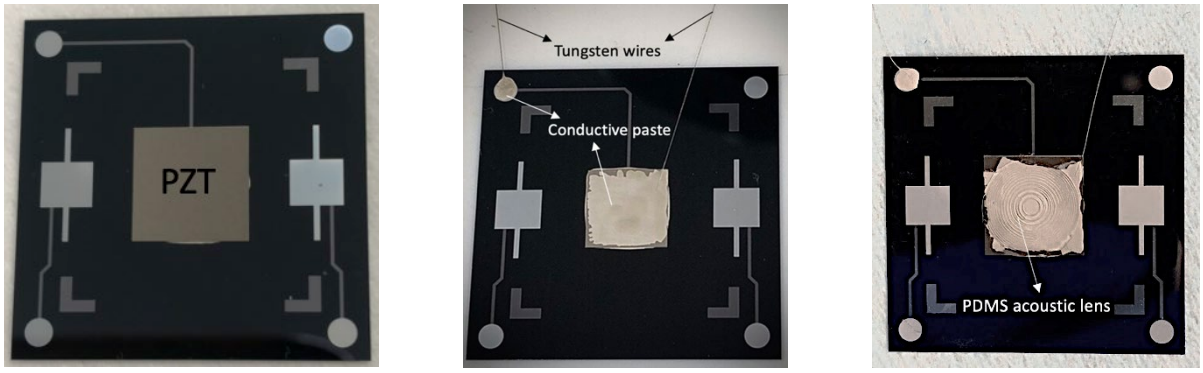

(a) (b) (c)

Figure 36 – Optical images of the test chip: (a) test chip with single PZT element, (b) test chip with tungsten wires and single PZT element covered with conductive paste, (c) PDMS acoustic Fresnel lens mounted on test chip.

3.7. Experimental measurement setup

The experimental setup makes use of the ultrasonic immersion technique, where the acoustic chip is placed in a DI water tank, as demonstrated in Figure 37. The emitter, i.e. the acoustic transducer (with acoustic Fresnel lens), is connected to a function generator (DG4202, RIGOL). A needle hydrophone (NH1000, Precision Acoustics), with a diameter of 1 mm and a sensitivity of 903 mV/Pa for frequency 16 MHz, is employed as receiver. A three-axis positioning stage (VK-62100, Gampt) is located inside the tank to align and position the hydrophone. The signal of the hydrophone is amplified (Precision Acoustics) and then read out by the oscilloscope (DSO-X 3032A, InfiniiVision). The oscilloscope is synchronized by a trigger signal from the function generator that matches the oscilloscope's measurement cycle with the input signal. The MATLAB software Experimental Visual Acoustics (EVA), developed in-house, was used for controlling the settings of the function generator, three-axis positioning stage and the oscilloscope. The software provided the ability to measure the acoustic output in different planes or in one axis for various acoustic parameter settings, such as the driving voltage and frequency.

A sinusoidal waveform is generated with a peak-to-peak amplitude of 10 V (V_{PP}). The frequency is set at 16 MHz and the burst number at 20. The generated acoustic output is presented in a 1D or 2D plot that consists of data points of the measured maximum peak-to-peak pressure. The measured maximum peak-to-peak pressure represents the temporal peak acoustic intensity (I_{SPTP}). The intensity of the acoustic signal is described by Equation (7), where p is the acoustic pressure, ρ the density of the medium and c the speed of sound in the medium.

(7) $$I = \frac{p^2}{\rho c}$$

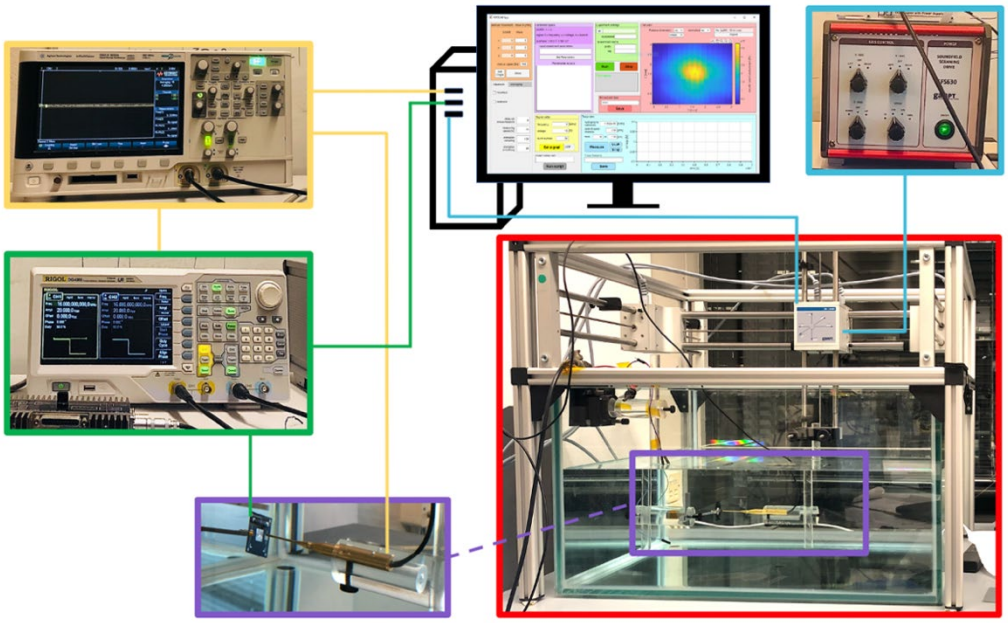

Figure 37 – Diagram of the experimental measurement setup: (red) DI water tank with three-axis positioning stage, (blue) three-axis stage controller, (purple) zoom-in of chip and needle hydrophone, (green) function generator, (yellow) oscilloscope, (black) computer with software EVA.

4. Results

The purpose of this work is to assess the performance of the acoustic PDMS Fresnel lenses designed to have a focal length of 6.5 – 7 mm for transducer frequencies 16 MHz and 12 MHz. This chapter presents the outcomes of the experimental measurements. The outcomes will be analysed and compared to the reference measurements, i.e. measurements obtained from the transducers without acoustic Fresnel lens. All measurements were performed using the setup described in Chapter 3.7 and the MATLAB software EVA. Measurements are done for the 6x6 mm and 10x10 mm acoustic Fresnel lenses using a transducer frequency of 16 MHz. Due to time constraints, the acoustic Fresnel lenses designed for transducer frequency 12 MHz were not examined.

4.1. Intensity profiles of the 6x6 mm acoustic Fresnel lens

First, measurements are conducted for the ultrasound transducer without using the designed acoustic Fresnel lens on top. Figure 38 shows the acoustic intensity perpendicular to the transducer at 7 mm distance from the 16 MHz transducer. From Figure 38a, it can be observed that the acoustic intensity profile for the transducer without acoustic lens shows dispersion of the acoustic waves without focusing at one point. The acoustic intensity profile of the transducer with acoustic lens is provided in Figure 38b. When the 6x6 mm acoustic Fresnel lens is mounted on the 6x6 mm transducer, the ultrasound waves are focused at 7 mm distance from the center of the transducer with a maximum peak-to-peak pressure of 1.46×10^4 Pa.

The focal length, f, of a transducer is given by Equation 7, where d is the diameter of the transducer and λ is the wavelength of the ultrasound beam propagating through the medium.

$$f = \frac{d^2}{4\lambda} \tag{7}$$

The measured acoustic intensity of the transducer without lens is higher compared to the acoustic intensity of the transducer with lens. However, using Equation (7), the natural focal length of the 16 MHz transducer without lens is at 93 mm distance from the transducer with a maximum peak-to-peak pressure of 1.3×10^4 Pa, as shown in Figure 39. From this it can be concluded that at 7 mm distance from the transducer, the ultrasound is still in the close near field where the acoustic pressure shows unpredictable behavior as it goes through many maxima and minima.

To determine the focus spot size, i.e. the width and the length of the focus spot, the FWHM is measured perpendicular and parallel to the transducer at 7 mm distance from the center of the transducer. The width of the focus spot is equal to the FWHM acquired by the acoustic intensity perpendicular to the transducer, which is 0.88 mm, as shown in Figure 40. Figure 41 presents the acoustic intensity parallel to the transducer, measured from 5 mm to 25 mm distance to center of the transducer, when no acoustic lens is employed. As can be observed from Figure 41, the acoustic waves are not focused within the given distance. Figure 42 presents the acoustic intensity parallel to the transducer with acoustic lens, measured from 5 mm to 70 mm distance to the center of the transducer. It can be seen that the highest intensity is found at 7 mm distance from the transducer, which matches the pre-determined focal length. The intensity decreases when the distance from the center of the transducer increases.

The length of the focus spot is 2.2 mm and is acquired by the FWHM of the acoustic intensity parallel to the transducer at 7 mm distance from the transducer, as demonstrated in Figure 42.

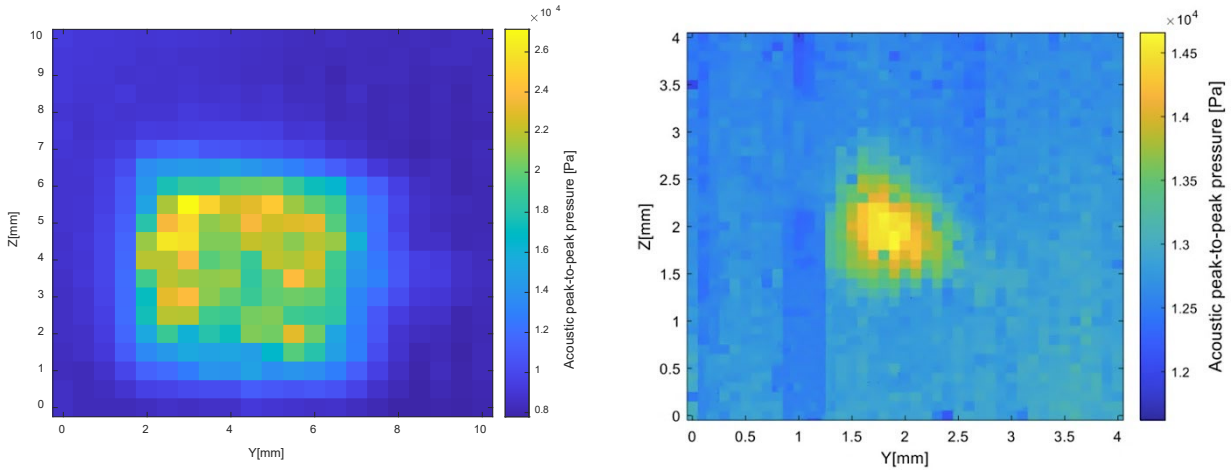

Figure 38 - 2D acoustic intensity profiles perpendicular to the transducer at 7 mm distance from the transducer: (a) without acoustic lens, (b) with acoustic lens. The ultrasound frequency is 16 MHz.

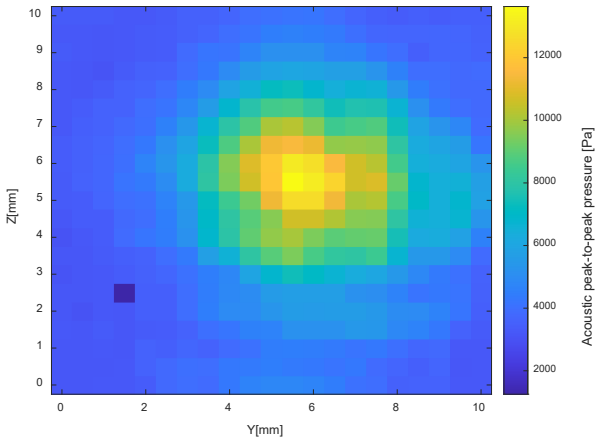

Figure 39 - 2D acoustic intensity profile, perpendicular to the transducer without acoustic lens, measured at a focal length of 93 mm. The ultrasound frequency is 16 MHz.

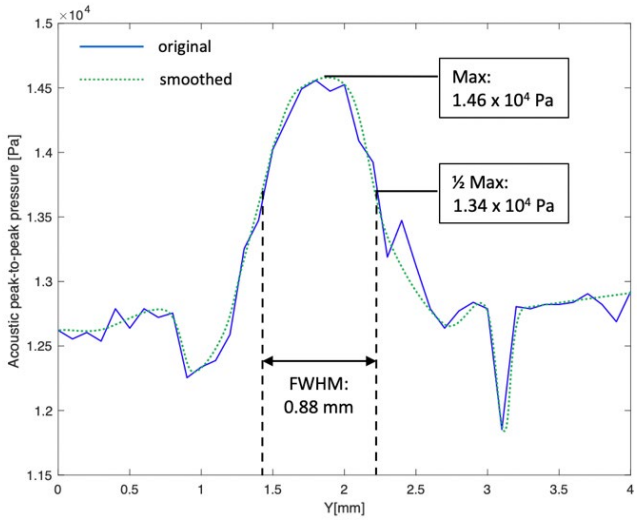

Figure 40 - 1D acoustic intensity profile, perpendicular to the 16 MHz transducer with acoustic lens, at 7 mm distance from the transducer. The width of the focus spot is 0.88 mm.

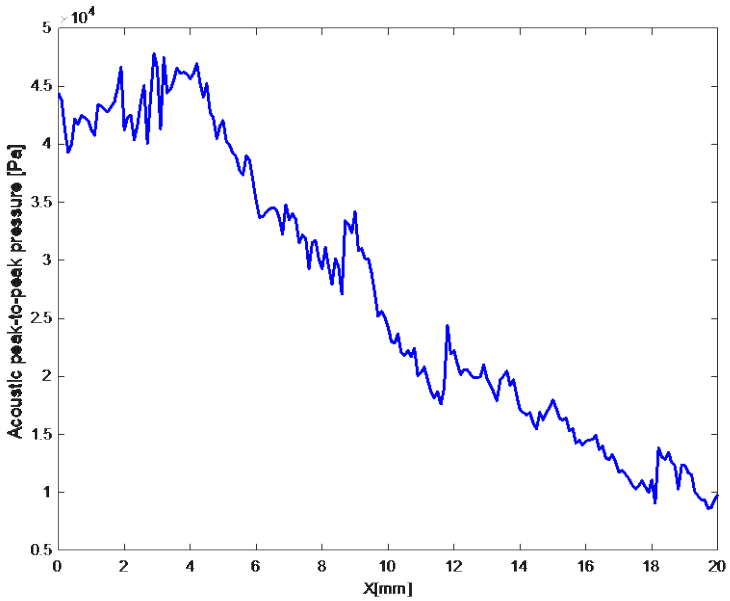

Figure 41 – 1D acoustic intensity profile, parallel to the 16 MHz transducer, measured from 5 – 25 mm distance to the center of the transducer. No acoustic lens is used.

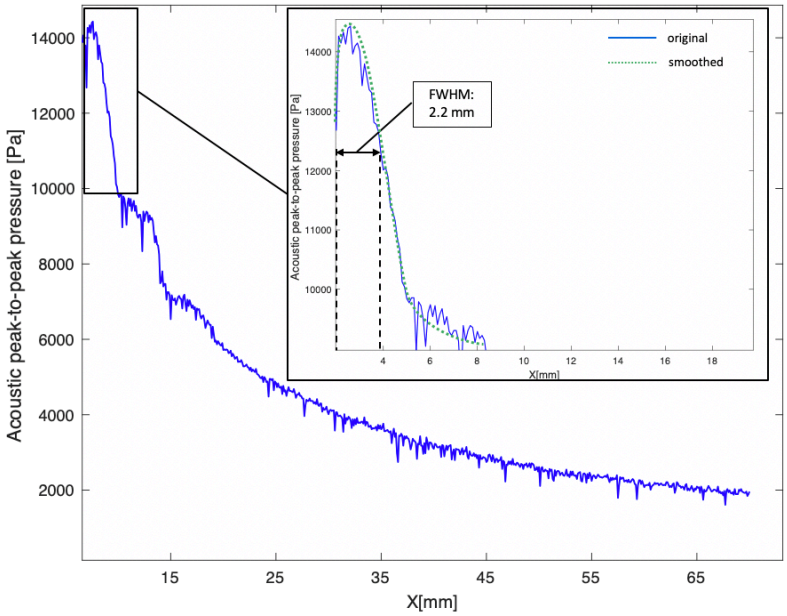

Figure 42 – 1D acoustic intensity profile, parallel to the 16 MHz transducer with acoustic lens, measured from 5 – 70 mm distance to the center of the transducer.
The length of the focus spot is 2.2 mm.

4.2. Intensity profiles of the 10x10 mm acoustic Fresnel lens

A 10x10 mm acoustic Fresnel lens is used on top of a 10x10 mm 16 MHz transducer to determine whether a greater number of zones in the acoustic lens, while preserving the frequency (16 MHz), will result in an improved focusing gain. Figure 43a shows the acoustic intensity perpendicular to the transducer at 7 mm distance from the transducer without acoustic lens. As can be observed from Figure 43a, there is no focus at the center of the transducer. The acoustic intensity perpendicular to the transducer with acoustic lens is shown in Figure 43b. Using the acoustic Fresnel lens on top of the transducer results in focusing the ultrasound beam at 7 mm from the center of the transducer with a maximum peak-to-peak pressure of 1.52×10^4 Pa. The measured acoustic intensity of the transducer without lens is higher compared to the acoustic intensity of the transducer with lens. From Equation (7) it can be calculated that the natural focal length of the transducer without acoustic lens is at 260 mm distance from transducer. The focal length of 260 mm is out of range of the water tank and hence, the acoustic intensity could not be measured at this distance. Instead, the acoustic intensity is measured at 100 mm distance from the transducer, as shown in Figure 44. From Figure 44 it can be observed that the ultrasound waves are not focused at one point and the ultrasound beam is still in near field. For this reason, the high intensity measured at 7 mm distance can be explained by the acoustic waves being in the close near field area.

The size of the focus spot is determined by the FWHM's measured perpendicular and parallel to the transducer at 7 mm distance from the center of the transducer. Figure 45 shows the width of the focus spot, which is equal to 0.85 mm. Figure 46 presents the acoustic intensity parallel to the transducer, measured from 5 mm to 25 mm distance to the transducer, when no acoustic lens is employed. As can be observed from Figure 46, the acoustic waves are not focused at one point within the given distance. Figure 47 illustrates the acoustic intensity parallel to the transducer measured from 5 mm to 100 mm distance to the center of the transducer. The acoustic lens focuses the ultrasound beam at 7 mm distance from the transducer with high intensity. As the distance from the center of the transducer increases, the intensity decreases. The length of the focus spot is calculated by the FWHM of the acoustic intensity parallel to the transducer at 7 mm distance from the transducer and is equal to 2.0 mm, as illustrated in Figure 47.

Table 7 compares the focus spot characteristics of the fabricated 6x6 mm and 10x10 mm acoustic Fresnel lenses designed for transducer frequency 16 MHz. An increase in the number of zones resulted in a smaller focus spot size. However, the difference is not significant. In Table 8, the focus spot characteristics derived from the COMSOL Multiphysics® simulations of the 5x5 mm and 10x10 mm acoustic Fresnel lenses are summarized. The simulations showed a decrease of approximately 38% in the width of the focus spot and a decrease of approximately 56% in the length of the focus spot when a 10x10 acoustic Fresnel lens is employed. These percentages are significantly larger compared to the difference found in the focus spot size between the fabricated 5x5 mm and the 10x10 mm acoustic Fresnel lenses.

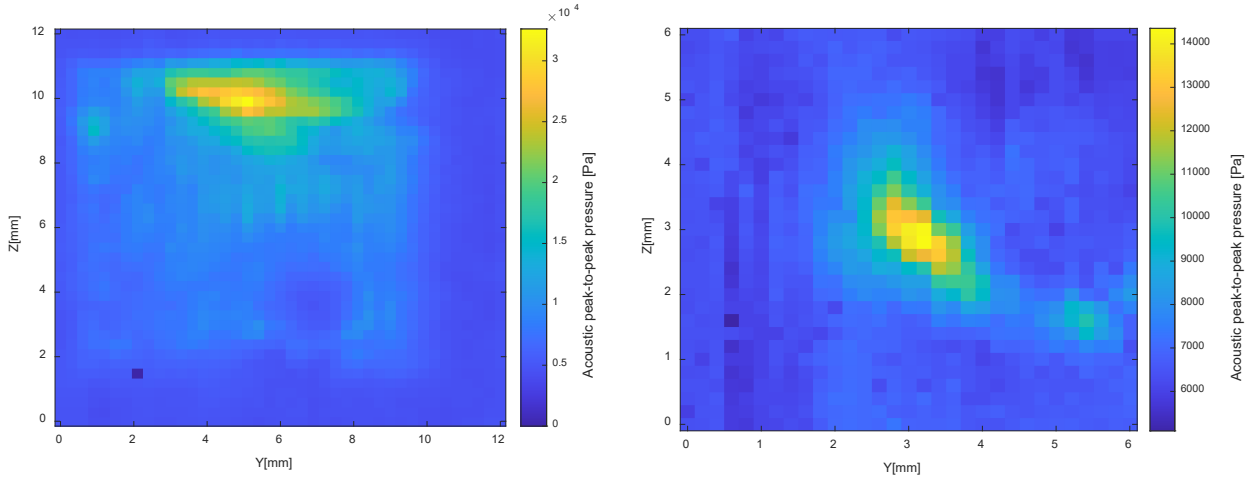

Figure 43 - 2D acoustic intensity profiles, perpendicular to the transducer at 7 mm distance from the transducer: (a) without acoustic lens, (b) with acoustic lens. The ultrasound frequency is 16 MHz.

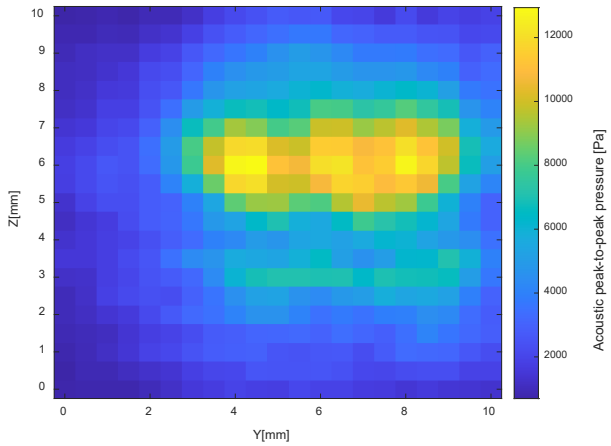

Figure 44 - 2D acoustic intensity profile, perpendicular to the transducer without acoustic lens, at 100 mm distance from the transducer.

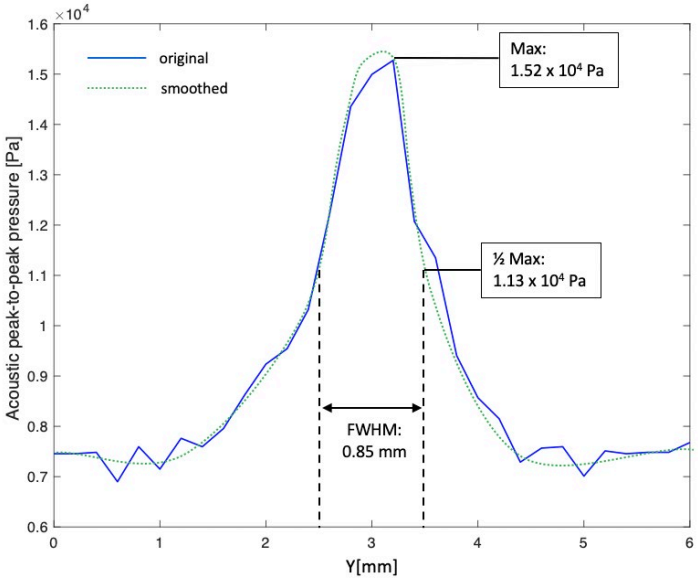

Figure 45 - 1D acoustic intensity profile, perpendicular to the 16 MHz transducer with acoustic lens, at 7 mm distance from the transducer. The width of the focus spot is 0.85 mm.

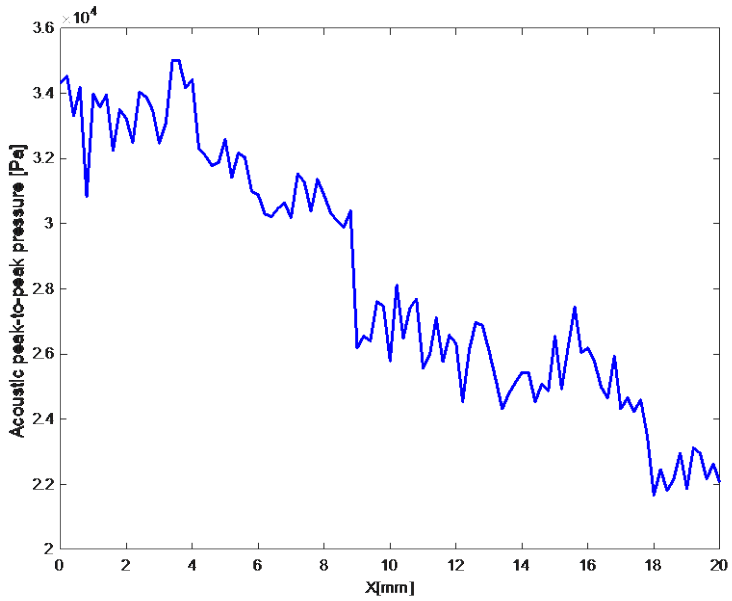

Figure 46 – 1D acoustic intensity profile, parallel to the 16 MHz transducer, measured from 5 – 25 mm distance to the center of the transducer. No acoustic lens is used.

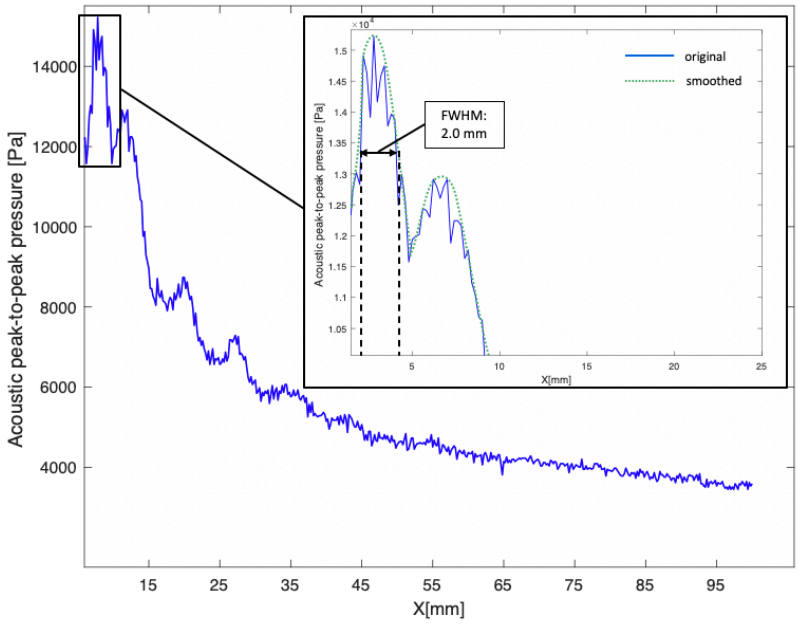

Figure 47 - 1D acoustic intensity profile, parallel to the 16 MHz transducer with acoustic lens, measured from 5 – 100 mm distance to the center of the transducer.
The length of the focus spot is 2.2 mm.

	6x6 mm	10x10 mm
Focal length (mm)	7.0	7.0
Width of focus spot (µm)	880	850
Length of focus spot (µm)	2200	2000

Table 7 – Characteristics of the focus spot derived from the outcomes of the experimental measurements: (a) 6x6 mm acoustic Fresnel lens, (b) 10x10 mm acoustic Fresnel lens. The transducer frequency is 16 MHz.

	6x6 mm	10x10 mm
Focal length (mm)	6.7	6.7
Width of focus spot (µm)	112	70
Length of focus spot (µm)	919	406

Table 8 – Characteristics of the focus spot derived from the COMSOL Multiphysics® simulations: (a) 6x6 mm acoustic Fresnel lens, (b) 10x10 mm acoustic Fresnel lens. The transducer frequency is 16 MHz.

5. Discussion

This chapter presents the limitations in the design and the fabrication of the acoustic Fresnel lenses. In addition, possible improvements of the cap structure will be briefly discussed. This is followed by describing the differences in the conditions used for the performed simulations and the experimental measurements. Finally, the experimental outcomes are interpreted with a focus on the focal length, focal pressure and the focal spot size.

5.1. Design acoustic lens

The design of the two-phase levels acoustic Fresnel lens is based on the radial distances and the step height that correspond to a given focal length and wavelength. From literature study and the simulations, it can be concluded that an increase in the number of zones will increase the focusing gain and decrease the focal spot size. Increasing the number of zones can be achieved by increasing the transducer frequency or the transducer diameter. It should be noted here that increasing the number of zones, will result in smaller features sizes, which are more prone to manufacturing errors. For *in vitro* studies focused on transcranial ultrasound neuromodulation, the frequency is limited due to skull attenuation. Studies that are focused on *in vitro* purposes only, can utilize a wide frequency range, going up to 1 GHz. For a given focal length and transducer diameter, the outer radius of the lens limits the total number of zones. Therefore, a trade off should be made between the transducer size and the number of zones.

5.2. Fabrication acoustic lens

The fabrication of the acoustic Fresnel lenses is based on standard photolithography methodologies, wet chemical processing and dry-etching processes. From the comparison between the designed and fabricated acoustic Fresnel lenses, it can be observed that the acoustic lens with a larger number of zones was more prone to fabrication errors due to smaller features. These fabrication errors are mostly caused by under etching during the isotropic wet etching step in the fabrication process. Small features (width of outer radius) require more wet etching time compared to larger features (width of inner radius) to allow the etchant to get to the surface of the to be etched layer. This results in loss of critical dimensions during DRIE. One possible solution is to compensate for this loss in the design of the photomask. An alternative is to use positive photoresist instead of negative photoresist. Positive photoresists can be spin coated up to 8 times thicker than negative photoresists [68]. Furthermore, the selectivity of positive photoresist (Photoresist:Si, 1:150) is high enough to be used in DRIE for the fabrication of the silicon mold [69]. The proposed method makes it possible to eliminate the wet etching step in the fabrication process and reduce the risk of manufacturing errors for small features, such as under etching.

5.3. Alignment of the lens

The fabricated acoustic Fresnel is manually aligned and mounted on the test chip, providing the advantage of realignment when the lens is not correctly placed. However, with each realignment, dust or dirt particles can build up underneath the lens. These particles result in the formation of air bubbles between the transducer and the lens, which can highly influence the transmission of ultrasound and decreases the diffraction efficiency of the lens.

Furthermore, if the adhesion between the acoustic lens and the transducer is poor, air can more easily penetrate. When the acoustic PDMS lens was manually attached to the cap structure, it could be observed that the formation of air bubbles was much lower compared to when the lens was attached to the parylene-coated PZT element on the test chip. A possible cause for this deviation is the surface roughness variation across the surface of the PZT element. Consequently, air can be easily trapped, resulting in the formation of air bubbles.

5.4. Cap structure

The cap structure is intended to be attached on top of the test chip, providing a top-level connection and a surface on which the lens can be placed. However, several problems were experienced during the fabrication and post-processing of the cap structure. Aluminum was used as conductive layer in the cap to provide a top-level connection to the PZT and closing the electric circuit. One major problem was the delamination of the PDMS layer. The aluminum layer started to be etched within the etch time that was required for fully removing the silicon dioxide layer in the cap. For this reason, the etching process could not be continued. The remaining silicon dioxide in the contact openings of the cap resulted in decreased conductivity. To overcome this problem, using a conductive metal with a longer etch time is essential to avoid delamination of the PDMS layer. From experiments using BHF (1:7), it was observed that titanium required an etching time of +20 minutes, whereas aluminum required an etch time of 14 minutes. Hence, titanium could be a good alternative to aluminum to be used in the cap.

5.5. Simulation and experimental conditions

There are several differences between the simulation and experimental conditions. First, the simulated model makes use of a circular transducer. The test chip used in the experimental measurements is square shaped. Furthermore, in the simulated model the backside of the transducer consists of an air gap to improve the transmission efficiency, which is not implemented in the test chip. In the simulations, an average value is taken for the density of PDMS. However, in reality, the density differs with the mixing ratio (monomer:curing agent) of PDMS. A difference in density will directly affect the acoustic impedance of PDMS.

5.6. Ultrasound intensity profiles

The 6x6 mm and 10x10 mm acoustic Fresnel lenses designed for transducer frequency 16 MHz are used for the experimental measurements. From the measured acoustic intensity profiles, it could be observed that the focal length of both lenses is 7.0 mm, which is in line with the simulations. However, the measured focus spot size is not comparable with the values found in the simulations. This discrepancy could come from the mismatch between the simulation conditions and the experimental conditions. One possible source is the use of a square shaped piezoelectric element in the experimental measurements. Ultrasound produced in the corners of the piezoelectric element did not contribute to the focusing effect of the lens. Consequently, this results in a lower ultrasound transmission through the lens. Using a circular transducer in the same diameter as the lens will increase the active area, which will lead to smaller values of the focus spot size. Comparing the 6x6 mm and 10x10 mm acoustic Fresnel lenses, an increase in the number of zones resulted in a smaller focus spot size. However, simulations have shown a significantly larger difference between the focus spot sizes when the number of zones is increased. In general, an acoustic lens with a larger number of zones will produce a smaller focus spot size, as the ultrasound beam is more tightly focused. However, the effect of the number of zones on focus spot size is not linear and depends on other factors, such as the

frequency and the lens geometry. An important factor that could affect the focus spot size is the accuracy of the radial distances between the zones. The smallest feature of the fabricated 10x10 mm acoustic Fresnel lens showed a deviation of approximately 10% with the designed lens. As a result, the diffraction of the acoustic waves is altered and could therefore lead to a larger spot size. Despite the fact that an increase in the number of zones resulted in a slightly smaller focus spot size, the difference is considered as not significant as a result of the fabrication errors. The 6x6 mm and 10x10 mm acoustic Fresnel lenses showed spatial-peak temporal-peak pressures of 14.6 kPa and 15.2 kPa, respectively. The more zones the acoustic lens has, the more the ultrasound energy is focused, resulting in higher intensities at the focus spot. Nevertheless, the measured pressures are not high enough for *in vitro* neuromodulation. The pressure levels required for *in vitro* neuromodulation are in the range of 0.1 to 1 MPa [1, 30, 70]. As aforementioned, the acoustic output can be increased by using a circular transducer with the same diameter as the lens. Another option is to drive the transducer with a higher voltage.

6. Conclusion

This thesis showed the design and fabrication of an acoustic PDMS lens on an ultrasound transducer to focus ultrasound for *in vitro* neuromodulation. The goal of this work was to focus the ultrasound waves with high spatial resolution at a pre-determined focal length (6.5 – 7 mm) to fit into the currently used MEA devices. The design of the acoustic lens was based on Fresnel lenses. Employing microfabrication technologies, a silicon mold was used for the fabrication of PDMS acoustic Fresnel lenses with different dimensions (6x6, 8x8 and 10x10 mm). Chips with a single bulk PZT element that matches the diameter of the acoustic Fresnel lens and with resonance frequency 16 MHz were used as ultrasound transducers. The focal length, focal spot size and intensities at the focal spot were examined to assess the performance of the acoustic lens. Furthermore, the effect of an increased number of zones on the focus spot size is analysed. The outcomes of this study have been demonstrated for an underwater configuration. From the experimental measurements, it can be observed that the acoustic Fresnel lenses focus the ultrasound beam at a focal length of 7.0 mm, which is within the desired focal length and in line with the performed simulations. An increase in the number of zones resulted in a higher focal spot pressure and smaller focus spot size. Although the simulations confirm these results, the measured difference in focus spot size, when a lens with a higher number of zones is employed, is considered as not significant due to the observed fabrication errors in the smallest features of the 10x10 mm acoustic Fresnel lens. In summary, the number of zones in an acoustic Fresnel lens can have a notable impact on both the intensity and focus spot size of the ultrasound beam, but the exact effect will depend on several factors, such as the frequency and the lens geometry.

Overall, this study demonstrated that microfabricated acoustic Fresnel lenses were capable of effective mechanical focusing at a pre-determined focal length. In addition, the fabrication of the acoustic Fresnel lens requires less complex fabrication compared to other acoustic focusing methods, such as phased arrays and gradient cross-sectional acoustic lenses. Therefore, acoustic Fresnel lenses show promising potential for focusing ultrasound for *in vitro* neuromodulation. However, further research is needed to improve the intensity at the focus spot and to achieve a smaller focus spot size.

6.1. Future work

Maximizing the energy transmitted through the acoustic lens can be achieved through different methods. The backside of the used test chip was not provided by an air gap. The air gap on the backside will improve the transmission energy of the PZT. The acoustic impedance mismatch between air and PZT will result in more acoustic energy being transmitted into the medium. Another method is to employ a circular transducer in the same diameter as the lens. These two improvements can be easily included in the processes described in this work. To further improve the acoustic transmission efficiency of the ultrasound transducer, an acoustic matching layer can be added or the piezoelectric material can be changed to a more advanced piezoelectric material, such as lead magnesium niobate-lead titanate (PMN-PT), which is known for its high electromechanical coupling coefficient and low dielectric loss.

In this work, the effect of varying the operating frequencies on the focal length was not studied. Fuster et al. have shown that the focal length increases with the operating frequency [71]. This

could be of particular interest when shifting of the focal length is desired. For instance, the cell culture in the MEA has a certain thickness. Depending on this thickness, the focal length can be accurately controlled by changing the operating frequency. However, the focus spot size is directly affected by the operating frequency and thus, restricting the range of focal lengths. Further research on shifting the focal length without losing spatial resolution is required. This would allow for more precise stimulation of the cell culture.

The acoustic PDMS Fresnel lenses can be easily reproduced as the silicon mold can be used repeatably for the production of the PDMS acoustic Fresnel lenses. Yet, the reproducibility can be further improved by carefully controlling the curing conditions and using a consistent mixing ratio of the PDNS monomer and curing agent. In addition, the throughput is low and curing of the PDMS is time-consuming. Curing at higher temperatures can accelerate the curing process, allowing for faster production times. However, the mechanical properties of PDMS are altered at higher temperatures and curing at higher temperatures can cause the PDMS to shrink or degrade, potentially affecting the accuracy of the final product [72,73]. Increasing time-efficiency and achieving large scale production for PDMS acoustic Fresnel lenses can be a challenging due to the limitations of the PDMS material. Injection Moulding (IM) or Injection Compression Moulding (ICM) are both process technologies that enable large scale production, where ICM leads to a higher dimensional accuracy of microstructures and surface quality [74]. Thermoplastic materials are commonly employed for IM and ICM. This makes PDMS, which is a thermoset polymer, an unsuitable material to be used in IM and ICM. For enabling a high throughput production of acoustic Fresnel lenses in the future, there is a need in finding a thermoplastic material that matches the mechanical and acoustic properties of PDMS.

References

1. Tyler, W., Tufail, Y., Finsterwald, M., Tauchmann, M., Olson, E., & Majestic, C. (2008). Remote Excitation of Neuronal Circuits Using Low-Intensity, Low-Frequency Ultrasound. *Plos ONE*, *3*(10), e3511.
2. Tyler, W., Lani, S., & Hwang, G. (2018). Ultrasonic modulation of neural circuit activity. *Current Opinion In Neurobiology*, *50*, 222-231.
3. Lee, W., Yoo, S., Jung, J., Kang, W., Wang, W., Moon, C., & Choi, H. (2017). All-in-one low-intensity pulsed ultrasound stimulation system using piezoelectric micromachined ultrasonic transducer (pMUT) arrays for targeted cell stimulation. *Biomedical Microdevices*, *19*(4).
4. Lee, W., Kim, H., Jung, Y., Chung, Y., Song, I., Lee, J., & Yoo, S. (2016). Transcranial focused ultrasound stimulation of human primary visual cortex. *Scientific Reports*, *6*(1).
5. Chen, H., Zhu, N., Osman, M., Biskowitz, R., Liu, J., & Khandare, S. et al. (2021). A transparent low intensity pulsed ultrasound (LIPUS) chip for high-throughput cell stimulation. *Lab On A Chip*, *21*(24), 4734-4742.
6. Fomenko, A., et al. (2018). "Low-intensity ultrasound neuromodulation: An overview of mechanisms and emerging human applications." Brain Stimulation 11(6): 1209
7. Padilla, F., Puts, R., Vico, L., & Raum, K. (2014). Stimulation of bone repair with ultrasound: A review of the possible mechanic effects. *Ultrasonics*, *54*(5), 1125-1145.
8. Kang, W., Jung, J., Lee, W., Ryu, J., & Choi, H. (2018). A thickness-mode piezoelectric micromachined ultrasound transducer annular array using a PMN–PZT single crystal. *Journal Of Micromechanics And Microengineering*, *28*(7), 075015.
9. Akhbari, S., Sammoura, F., Yang, C., Mahmoud, M., Agab, N., & Lin, L. (2015). Bimorph pMUT with dual electrodes. *2015 28th IEEE International Conference on Micro Electro Mechanical Systems (MEMS)*, pp. 928-931.
10. Bushberg, J. (2012). *The essential physics of medical imaging*. Philadelphia, PA: Wolters Kluwer / Lippincott Williams & Wilkins.
11. Ozevin, D., et al. (2005). Adapting a cMUT transducer to detect acoustic emissions. *IEEE Ultrasonics Symposium,* pp. 956-959.
12. Jung, J., Lee, W., Kang, W., Shin, E., Ryu, J., & Choi, H. (2017). Review of piezoelectric micromachined ultrasonic transducers and their applications. *Journal Of Micromechanics And Microengineering*, *27*(11), 113001.
13. Sammoura, F., Akhbari, S., Lin, L. (2016). Piezoelectric transducers and methods of making and using the same. U.S. Patent Application No. PCT/US20 16/0 13432. California, U.S: World Intellectual Property Organization (WIPO), The Patent Cooperation Treaty (PCT).
14. Shin, E., Yeo, H., Yeon, A., Jin, C., Park, W., Lee, S., & Choi, H. (2020). Development of a High-Density Piezoelectric Micromachined Ultrasonic Transducer Array Based on Patterned Aluminum Nitride Thin Film. *Micromachines*, *11*(6), 623.
15. Qiu, Y., Gigliotti, J., Wallace, M., Griggio, F., Demore, C., Cochran, S., & Trolier-McKinstry, S. (2015). Piezoelectric Micromachined Ultrasound Transducer (PMUT) Arrays for Integrated Sensing, Actuation and Imaging. *Sensors*, *15*(4), 8020-8041.
16. Khuri-Yakub, B., & Oralkan, Ö. (2011). Capacitive micromachined ultrasonic transducers for medical imaging and therapy. *Journal Of Micromechanics And Microengineering*, *21*(5), 054004.
17. Oralkan, O., Bayram, B., Yaralioglu, G., Ergun, A., Kupnik, M., & Yeh, D. et al. (2006). Experimental characterization of collapse-mode CMUT operation. *IEEE Transactions On Ultrasonics, Ferroelectrics And Frequency Control*, *53*(8), 1513-1523.
18. Bayram, B., Haeggstrom, E., Yaralioglu, G., & Khuri-Yakub, B. (2003). A new regime for operating capacitive micromachined ultrasonic transducers. *IEEE Transactions On Ultrasonics, Ferroelectrics And Frequency Control*, *50*(9), 1184-1190.

19. Salim, M., Abd Malek, M., Heng, R., Juni, K., & Sabri, N. (2012). Capacitive Micromachined Ultrasonic Transducers: Technology and Application. *Journal Of Medical Ultrasound*, *20*(1), 8-31.
20. Yaralioglu, G., Ergun, A., Bayram, B., Haeggstrom, E., & Khuri-Yakub, B. (2003). Calculation and measurement of electromechanical coupling coefficient of capacitive micromachined ultrasonic transducers. *IEEE Transactions On Ultrasonics, Ferroelectrics And Frequency Control*, *50*(4), 449-456.
21. Hwang, G., Park, H., Lee, J., Oh, S., Park, K., & Byun, M. et al. (2014). Self-Powered Cardiac Pacemaker Enabled by Flexible Single Crystalline PMN-PT Piezoelectric Energy Harvester. *Advanced Materials*, *26*(28), 4880-4887.
22. Muralt, P., Ledermann, N., Paborowski, J., Barzegar, A., Gentil, S., & Belgacem, B. et al. (2005). Piezoelectric micromachined ultrasonic transducers based on PZT thin films. *IEEE Transactions On Ultrasonics, Ferroelectrics And Frequency Control*, *52*(12), 2276-2288.
23. Cho, J., Anderson, M., Richards, R., Bahr, D., & Richards, C. (2005). Optimization of electromechanical coupling for a thin-film PZT membrane: I. Modeling. *Journal Of Micromechanics And Microengineering*, *15*(10), 1797-1803.
24. Akhbari, S., Sammoura, F., Eovino, B., Yang, C., & Lin, L. (2016). Bimorph Piezoelectric Micromachined Ultrasonic Transducers. *Journal Of Microelectromechanical Systems*, *25*(2), 326-336.
25. Hajati, A., Latev, D. & Gardner, D. 3D MEMS piezoelectric ultrasound transducer technology. *2013 Joint IEEE International Symposium on Applications of Ferroelectric and Workshop on Piezoresponse Force Microscopy (ISAF/PFM)*, 2013, pp. 231-235.
26. Chen, H., Zhu, N., Osman, M., Biskowitz, R., Liu, J., & Khandare, S. et al. (2021). A transparent low intensity pulsed ultrasound (LIPUS) chip for high-throughput cell stimulation. *Lab On A Chip*, *21*(24), 4734-4742.
27. Lee, W., Yoo, S., Jung, J., Kang, W., Wang, W., Moon, C., & Choi, H. (2017). All-in-one low-intensity pulsed ultrasound stimulation system using piezoelectric micromachined ultrasonic transducer (pMUT) arrays for targeted cell stimulation. *Biomedical Microdevices*, *19*(4).
28. Kang, W., Jung, J., Lee, W., Ryu, J., & Choi, H. (2018). A thickness-mode piezoelectric micromachined ultrasound transducer annular array using a PMN–PZT single crystal. *Journal Of Micromechanics And Microengineering*, *28*(7), 075015.
29. Lee, J., Ko, K., Shin, H., Oh, S., Lee, C., & Chou, N. et al. (2019). A MEMS ultrasound stimulation system for modulation of neural circuits with high spatial resolution in vitro. *Microsystems & Nanoengineering*, *5*(1).
30. Choi, J. B., Lim, S. H., Cho, K. W., Kim, D. H., Jang, D. P., & Kim, I. Y. (2013). The effect of focused ultrasonic stimulation on the activity of hippocampal neurons in multi-channel electrode. *2013 6th International IEEE/EMBS Conference on Neural Engineering (NER)*, 731-734.
31. Kim, H., Swanberg et al. (2016). Prolonged stimulation with low-intensity ultrasound induces delayed increases in spontaneous hippocampal culture spiking activity. *Journal of Neuroscience Research, 95*(3), 885-896.
32. Khraiche, M. L., Phillips, W. B., Jackson, N., & Muthuswamy, J. (2008). Ultrasound induced increase in excitability of single neurons. *2008 30th Annual International Conference of the IEEE Engineering in Medicine and Biology Society*, 4246-4249
33. Ma, F., Huang, Z., Liu, C., & Wu, J. (2022). Acoustic focusing and imaging via phononic crystal and acoustic metamaterials. *Journal Of Applied Physics*, *131*(1), 011103.
34. Yong-Qi, F., Kok Ann Bryan, N., & Shing, O. (2000). Diffractive optical elements with continuous relief fabricated by focused ion beam for monomode fiber coupling. *Optics Express*, *7*(3), 141.
35. Pérez-López, S., Fuster, J., & Candelas, P. (2019). M-Bonacci Zone Plates for Ultrasound Focusing. *Sensors*, *19*(19), 4313.

36. Bui, Anh & Pan, Min-Chun & Wu, Tzon-Han & Le, Thanh Long. (2020). Using SiO2 Hard Mask for Fabrication of Micro Fresnel Focusing Lens for Ultrasonic Ejectors. *Key Engineering Materials 863.*
37. Bui, T., & Pan, M. (2017). Focusing efficiency evaluation of ultrasonic energy for fabricated Fresnel lens through surface profile estimation and FEA. *Ferroelectrics*, *506*(1), 76-92.
38. Hadimioglu, B. & Rawson, E.G. & Lujan, Renaldo & Lim, M. & Zesch, James & Khuri-Yakub, Pierre & Quate, C.F.. (1993). High-efficiency Fresnel acoustic lenses. pp.579 – 582, vol.1.
39. Shin Chuen Chan, Mina, M., Udpa, S., Udpa, L., & Lord, W. (1996). Finite element analysis of multilevel acoustic Fresnel lenses. *IEEE Transactions On Ultrasonics, Ferroelectrics And Frequency Control*, *43*(4), 670-677.
40. Alda, J., Rico-García, J., López-Alonso, J., Lail, B., & Boreman, G. (2006). Design of Fresnel lenses and binary-staircase kinoforms of low value of the aperture number. *Optics Communications*, *260*(2), 454-461.
41. Pan, M., Bui, T., Nien, Y., & Shih, W. (2011). Design and Fabrication of Fresnel Lens and ZnO Thin-Film Transducer. *Japanese Journal Of Applied Physics*, *50*(7S), 07HD02.
42. Li, J., Craig, F., & Keynton, R. (2002). Design and fabrication of a miniaturized, integrated, high-frequency acoustical lens–transducer system. *Journal of Micromechanics and Microengineering*. *12.* 219.
43. Xia, W., Piras, D., van Hespen, J., Steenbergen, W., & Manohar, S. (2013). A new acoutic lens material for large area detectors in photoacoustic breast tomography. *Photoacoustics, 1(2),* 9-18.
44. Miranda, I., Souza, A., Sousa, P., Ribeiro, J., Castanheira, E., Lima, R., & Minas, G. (2021). Properties and Applications of PDMS for Biomedical Engineering: A Review. *Journal Of Functional Biomaterials*, *13*(1), 2.
45. Vázquez, R., Eaton, S., Ramponi, R., Cerullo, G., & Osellame, R. (2011). Fabrication of binary Fresnel lenses in PMMA by femtosecond laser surface ablation. *Optics Express*, *19*(12), 11597. doi: 10.1364/oe.19.011597
46. Willerth, S. (2017). *Engineering Neural Tissue from Stem Cells* (Chapter 6 - Synthetic biomaterials for engineering neural tissue from stem cells). London: Academic Press.
47. Tu, Y., Chen, S., & Hwang, Y. (2016). Design of Fresnel Lens-Type Multi-Trapping Acoustic Tweezers. *Sensors*, *16*(11), p.1973.
48. Destgeer, G., Jung, J., Park, J., Ahmed, H., Park, K., Ahmad, R., & Sung, H. (2017). Acoustic impedance-based manipulation of elastic microspheres using travelling surface acoustic waves. *RSC Advances*, *7*(36), 22524-22530.
49. Yunas, J., Mulyanti, B., Hamidah, I., Mohd Said, M., Pawinanto, R., & Wan Ali, W. et al. (2020). Polymer-Based MEMS Electromagnetic Actuator for Biomedical Application: A Review. *Polymers*, *12*(5), 1184.
50. Rahman, M.F.A. & Arshad, Mohd Rizal & Abd Manaf, Asrulnizam & Yaacob, M.I.H.. (2012). An investigation on the behaviour of PDMS as a membrane material for underwater acoustic sensing. *Indian Journal of Marine Sciences*. 41. 557-562.
51. Kim, M., Moon, B., & Hidrovo, C. (2013). Enhancement of the thermo-mechanical properties of PDMS molds for the hot embossing of PMMA microfluidic devices. *Journal Of Micromechanics And Microengineering*, *23*(9), 095024.
52. X. Li *et al.* (2015). Tunable binary Fresnel lens based on stretchable PDMS/CNT composite. *2015 Transducers - 2015 18th International Conference on Solid-State Sensors, Actuators and Microsystems (TRANSDUCERS)*, 2041-2044
53. Tang, Y., Liu S., & Kim, E.S. (2020). MEMS Focused Ultrasonic Transducer with Air-Cavity Lens Based on Polydimethylsiloxane (PDMS) Membrane. *2020 IEEE 33rd International Conference on Micro Electro Mechanical Systems (MEMS)*, pp. 58-61.
54. Chang, C., Firouzi, K., Kyu Park, K., Sarioglu, A., Nikoozadeh, A., Yoon, H., Vaithilingam, S., Carver, T. and Khuri-Yakub, B. (2014). Acoustic lens for capacitive micromachined ultrasonic transducers. *Journal of Micromechanics and Microengineering*, 24(8), p.085007.

55. Marczak, J., Slupski, P., Kunicki, P., & Komorowska, K. (2015). Soft lithography processing of fresnel lens for on-chip applications. *2015 IEEE 15th International Conference on Nanotechnology (IEEE-NANO)*, pp. 975-978.
56. Bani-Yaghoub, M., Tremblay, R., Voicu, R., Mealing, G., Monette, R., Py, C., Faid, K. and Sikorska, M. (2005). Neurogenesis and neuronal communication on micropatterned neurochips. *Biotechnol. Bioeng.,* 92: pp. 336-345.
57. Park, J., et al. (2012). Three-dimensional nanonetworks for giant stretchability in dielectrics and conductors. *Nat. Commun*., vol. 3, no. May, p. 916.
58. Gougheri, H., Dangi, A., Kothapalli, S., & Kiani, M. (2019). A Comprehensive Study of Ultrasound Transducer Characteristics in Microscopic Ultrasound Neuromodulation. *IEEE Transactions On Biomedical Circuits And Systems*, *13*(5), 835-847.
59. I. Wygant. (2011). A comparison of CMUTs and piezoelectric transducer elements for 2D medical imaging based on conventional simulation models. *IEEE International Ultrasonics Symposium*, 100-103.
60. Costa, T., Shi, C., Tien, K., Elloian, J., Cardoso, F., & Shepard, K. (2021). An Integrated 2D Ultrasound Phased Array Transmitter in CMOS With Pixel Pitch-Matched Beamforming. *IEEE Transactions On Biomedical Circuits And Systems*, *15*(4), 731-742.
61. Wang, Y., Tao, J., Guo, F., Li, S., Huang, X., Dong, J., & Cao, W. (2018). Magnesium Alloy Matching Layer for High-Performance Transducer Applications. *Sensors*, *18*(12), 4424.
62. Schuster, A., Schwab, T., Bischof, M., Klotz, M., Lemor, R., Degel, C., & Schäfer, K. (2013). Cell specific ultrasound effects are dose and frequency dependent. *Annals Of Anatomy - Anatomischer Anzeiger*, *195*(1), 57-67.
63. Balasubramanian, P., Singh, A., Xu, C., & Lal, A. (2020). GHz Ultrasonic Chip-Scale Device Induces Ion Channel Stimulation in Human Neural Cells. *Scientific Reports*, *10*(1).
64. Shin, S., Kim, N., Hong, J.W. (2018). Comparison of surface modification techniques on polydimethylsiloxane to prevent proteinadsorption. *BioChip J., 12,* 123–127.
65. Ren, K., Dai, W., Zhou, J., Su, J., & Wu, H. (2011). Whole-Teflon microfluidic chips. *Proceedings Of The National Academy Of Sciences*, *108*(20), 8162-8166.
66. Lou, K., Granick, S., & Amblard, F. (2018). How to better focus waves by considering symmetry and information loss. *Proceedings Of The National Academy Of Sciences*, *115*(26), 6554-6559.
67. Epoxy technology | EPO-Tek H20E - Datasheet PDF & Tech Specs. (n.d.). Retrieved December 15, 2023, from https://www.epotek.com/docs/en/Datasheet/H20E.pdf
68. Composition and properties of AZ® and TI photoresists |Technical information PDF – Photoresist composition properties. MicroChemicals GmbH (2019). Retrieved January 27, 2023, from https://www.microchemicals.com/technical_information/photoresists_composition_properties.pdf
69. Dry etching with photoresist masks | Technical information PDF – Dry etching. MicroChemicals GmbH (2019). Retrieved January 27, 2023, from https://www.microchemicals.com/technical_information/dry_etching_photoresist.pdf
70. Furukawa, R., Kaneta, H., & Tateno, T. (2022). A multielectrode array-based recording system for analyzing ultrasound-driven neural responses in brain slices in vitro. *Frontiers in Neuroscience*, *16*.
71. Fuster, J., Candelas, P., Castiñeira-Ibáñez, S., Pérez-López, S., & Rubio, C. (2017). Analysis of fresnel zone plates focusing dependence on operating frequency. *Sensors*, *17*(12), 2809.
72. Johnston, I. D., McCluskey, D. K., Tan, C. K., & Tracey, M. C. (2014). Mechanical characterization of bulk Sylgard 184 for microfluidics and microengineering. *Journal of Micromechanics and Microengineering*, *24*(3), 035017.
73. Lee, S. W., & Lee, S. S. (2007). Shrinkage ratio of PDMS and its alignment method for the wafer level process. *Microsystem Technologies*, *14*(2), 205–208.
74. Loaldi, D., Quagliotti, D., Calaon, M., Parenti, P., Annoni, M., & Tosello, G. (2018). Manufacturing signatures of injection molding and injection compression molding for micro-

Appendices

A. Design

r_k	value (mm)
r_1	900
r_2	1274
r_3	1562
r_4	1806
r_5	2022
r_6	2217
r_7	2398
r_8	2567
r_9	2726
r_{10}	2877
r_{11}	3021
r_{12}	3159
r_{13}	3292
r_{14}	3420
r_{15}	3545
r_{16}	3665
r_{17}	3782
r_{18}	3897
r_{19}	4008
r_{20}	4117
r_{21}	4224
r_{22}	4329
r_{23}	4431
r_{24}	4532
r_{25}	4631
r_{26}	4728
r_{27}	4824
r_{28}	4918

Radial distances for 8x8 mm acoustic Fresnel lens

Radial distances for 6x6 mm acoustic Fresnel lens

Radial distances for 10x10 mm acoustic Fresnel lens

Table A.1 - The calculated radial distances for the design of the two-phase levels acoustic Fresnel lenses for transducer frequency 12 MHz. Step height = 164 µm.

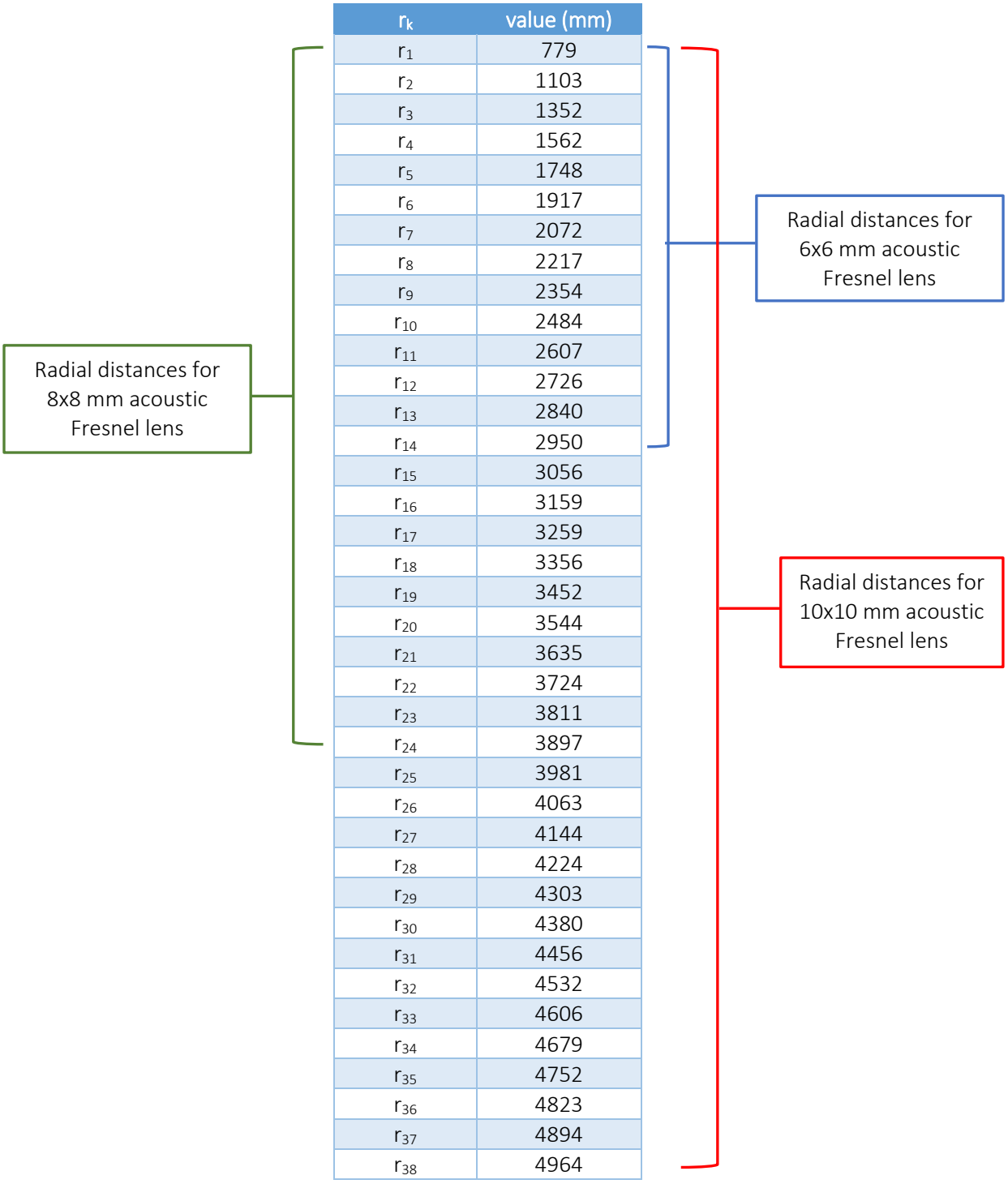

r_k	value (mm)
r_1	779
r_2	1103
r_3	1352
r_4	1562
r_5	1748
r_6	1917
r_7	2072
r_8	2217
r_9	2354
r_{10}	2484
r_{11}	2607
r_{12}	2726
r_{13}	2840
r_{14}	2950
r_{15}	3056
r_{16}	3159
r_{17}	3259
r_{18}	3356
r_{19}	3452
r_{20}	3544
r_{21}	3635
r_{22}	3724
r_{23}	3811
r_{24}	3897
r_{25}	3981
r_{26}	4063
r_{27}	4144
r_{28}	4224
r_{29}	4303
r_{30}	4380
r_{31}	4456
r_{32}	4532
r_{33}	4606
r_{34}	4679
r_{35}	4752
r_{36}	4823
r_{37}	4894
r_{38}	4964

Table A.2 – The calculated radial distances for the design of the two-phase levels acoustic Fresnel lenses for transducer frequency 16 MHz. Step height = 123 µm.

r_k	value (mm)
r_1	636
r_2	900
r_3	1103
r_4	1274
r_5	1425
r_6	1562
r_7	1688
r_8	1806
r_9	1917
r_{10}	2022
r_{11}	2122
r_{12}	2217
r_{13}	2309
r_{14}	2398
r_{15}	2484
r_{16}	2567
r_{17}	2647
r_{18}	2726
r_{19}	2802
r_{20}	2877

Table A.3 – The calculated radial distances for the design of the 3x3 mm multiphase levels acoustic Fresnel lenses for transducer frequency 12 MHz. Step height = 82 µm.

r_k	value (mm)
r_1	551
r_2	779
r_3	954
r_4	1103
r_5	1233
r_6	1352
r_7	1461
r_8	1562
r_9	1658
r_{10}	1748
r_{11}	1834
r_{12}	1917
r_{13}	1996
r_{14}	2072
r_{15}	2146
r_{16}	2217
r_{17}	2287
r_{18}	2354
r_{19}	2420
r_{20}	2484
r_{21}	2485
r_{22}	2546
r_{23}	2607
r_{24}	2667
r_{25}	2726
r_{26}	2783
r_{27}	2840
r_{28}	2895

Table A.4 – The calculated radial distances for the design of the 3x3 mm multiphase levels acoustic Fresnel lenses for transducer frequency 16 MHz. Step height = 62 µm.

B. Simulations

Setting	Value
Transducer radius	3 mm
Transducer thickness	0.15 mm for 12 MHz 0.11 mm for 16 MHz
Driving voltage	5 V
Mesh size	1480 (m/s) / frequency / 5
Minimum element size	3.66×10^{-6} µm
PDMS – density (ρ)	970 kg/m^3
PDMS – speed of sound (c)	1076.5 m/s
Piezoelectric material	PZT-5H

Table B.1 - The conditions used to perform the simulations in COMSOL Multiphysics.

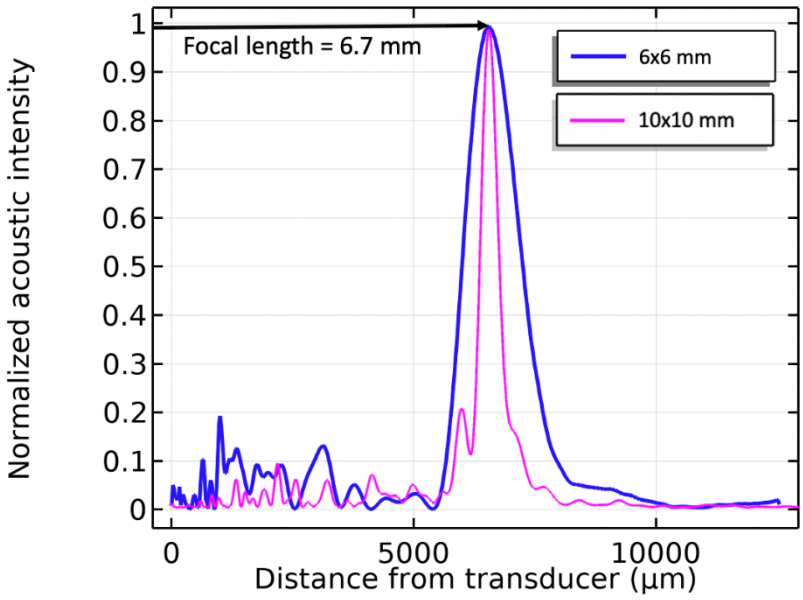

Figure B.1 – Comparison of the acoustic intensities, parallel to the transducer, between a 6x6 mm and 10x10 mm acoustic Fresnel lens on top of the transducer. The transducer frequency is 16 MHz.

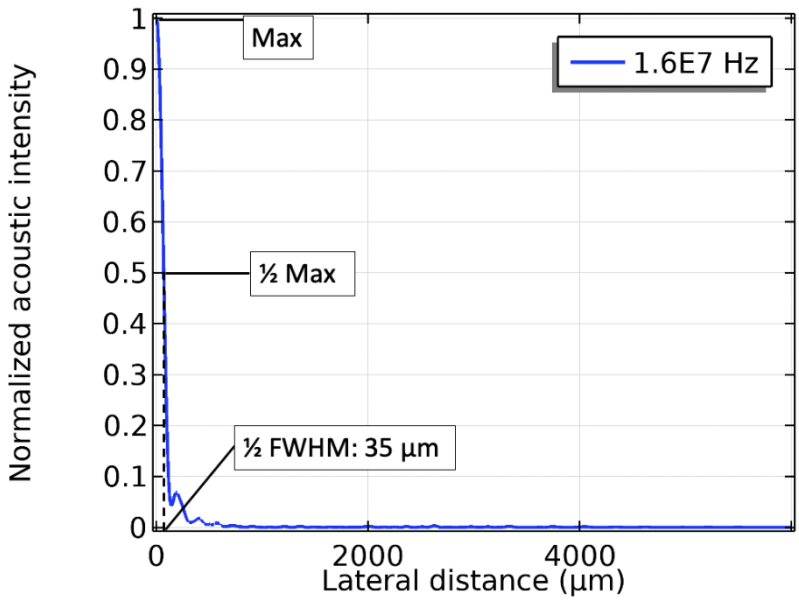

Figure B.2 – Acoustic intensity, perpendicular to the transducer, using a 10x10 mm acoustic Fresnel lens on top of the transducer.

C. Flowchart Microfabrication

STARTING MATERIAL

Use **SINGLE SIDE** polished **LOW RESISTIVITY (L_{RES})** wafers,
with the following specifications:

Type:	p
Orientation:	<100>
Resistivity:	1-5 Ωcm
Thickness:	525 ± 15 μm
Diameter:	100 mm

PECVD Oxide

1. PECVD DEPOSITION: 500 nm Silicon oxide

Use the Novellus Concept One PECVD reactor.
It is not allowed to change the process conditions and time from the deposition recipe!

Use recipe ".xxx_siostd" to deposit a 500 nm thick SiO2 layer.

Process conditions from recipe .xxx_siostd:					
Gasses & flows	Pressure	HF power	LF power	Temperature	Time
N2/SiH4/N2O = 3150/205/6000 sccm	2.2 Torr	1000 W	0 W	400 °C	variable

Note:

- The layer thickness depends on the station deposition time (SDT), which can be calculated from the average deposition rate during recent recipe usage. This can be found in the logbook of the system.
- An extra test wafer can be deposited for measurements and etch tests.

2. MEASUREMENT: oxide thickness

Use the Leitz MPV-SP measurement system for layer thickness measurements.

⇨ Use program: Th. SiO2 on Si, >50nm auto5pts

Expected layer thickness: 500 nm

Negative photoresist NLOF

3. COATING

Use the coater station of the EVG120 system to coat the wafers with photoresist.
Always check the relative humidity (48 ± 2 %) in the room before coating, and follow the instructions for this equipment.

Use program "SpeCo – Nlof – 3.5 um – no HDMS no EBR".

4. ALIGNMENT AND EXPOSURE

Use the EVG420 contact aligner

Note: Check the calibrated dosage before exposure time calculation
Note: Make sure to book a reservation for the system
Use box: XXX and mask: XXX for microwell and contact-pad openings
Expose the NLOF2020-soft-baked wafer:

- Use the Soft-Contact setting
- Put mask into mask holder (chrome side up), turn on its vacuum and clamp mechanically

- Place mask holder in machine, activate mask holder clamping and forcefully test rigidity
- Align the Mask's alignment markers
- Use the uncontaminated contact aligner chuck
- Place wafer onto wafer slide, turn on vacuum and test wafer attachment
- Align the wafer's alignment markers to the mask's alignment markers
- Set exposure time:

  Exposure_time =
  Required_dose (thickness dependent) / Dose_per_second (calibrated value next to machine) * Relative_dose

  3.5 um NLOF → i-line @ 80mJ/cm2 (80 mJ/cm2 / 2.7) x 1.1 = 32.6 sec

- Alignment check
- Expose
- Open wafer slide and then turn off vacuum
- Open mask holder clamp, remove mask holder, turn off mask holder vacuum and open mechanical clamp

5. DEVELOPING

Use the developer station of the EVG120 system to develop the wafers.
Always follow the instructions for this equipment.

Use program 'X-link bake' and then program "1-Dev – lift off".

6. INSPECTION

Visually inspect the wafers through a microscope:

- No resist residues are allowed.
- Check the linewidth of the structures.
- Check the overlay of the exposed pattern if the mask was aligned to a previous pattern on the wafer.

Wet etching of Oxide

BHF – green metals
Etch rate PECVD oxide and BHF: 250-300nm/min
Total etch time: 2min and 30 sec

7. Wet Etching Silicon oxide: 500nm (Etching line -- Si bath)

Moisten	Rinse for 1 minute in wet bench "H2O/Triton X-100 tbv BHF 1:7". Use the carrier with the blue dot. The bath contains 1 ml Triton X-100 per 5000 ml deionized water.
Etch	Use wet bench "BHF 1:7 (SiO2-ets) Si" at ambient temperature, and the carrier with the blue dot. The bath contains a buffered HF solution.
Time	Etch until the windows on the front side are hydrophobic, plus an extra 30 seconds. The required etch time depends on the layer thickness and composition.The etch rate of thermally grown oxide is 1.3 ± 0.2 nm/s at 20 °C.
Rinse	Rinse in the Quick Dump Rinser with the standard program until the resistivity is 5 MΩ.
Dry	Use the "Avenger Ultra-Pure 6" rinser/dryer with the standard program, and the white carrier with a black dot.
Inspection	Visually, through a microscope: All the windows must be open and the hydrophobic test may be applied.

8. CLEANING PROCEDURE: TEPLA + HNO3 100% and 65% for green metals

Plasma strip	Use the Tepla plasma system to remove the photoresist in an oxygen plasma. Follow the instructions specified for the Tepla stripper and use the quartz carrier. Use program 1
Cleaning	10 minutes in fuming nitric acid (Merck: HNO3 100%) at ambient temperature. Use wet bench "HNO3 (100%) green metls" and the carrier with the red dot.
QDR	Rinse in the Quick Dump Rinser with the standard program until the resistivity is 5 MΩ.
Cleaning	10 minutes in concentrated nitric acid (Merck: HNO3 65%) at 110 °C. Use wet bench "HNO3 (65%)" and the carrier with the red dot.
QDR	Rinse in the Quick Dump Rinser with the standard program until the resistivity is 5 MΩ.
Drying	Use the Semitool "rinser/dryer" with the standard program, and the white carrier with a red dot.

Si Etching

9. PLASMA ETCHING SILICON (100 to 300um)

Use the Rapier Omega i2L DRIE etcher.
Follow the operating instructions from the manual when using this machine.
Recipe: 0_EKL_SMOOTH_20C_XX

Number of cycles depend on the etching depth.

10. CLEANING PROCEDURE: HNO3 100% and 65% for green metals

Cleaning	10 minutes in fuming nitric acid (Merck: HNO3 100%) at ambient temperature. Use wet bench "HNO3 (100%) green metls" and the carrier with the red dot.
QDR	Rinse in the Quick Dump Rinser with the standard program until the resistivity is 5 MΩ.
Cleaning	10 minutes in concentrated nitric acid (Merck: HNO3 65%) at 110 °C. Use wet bench "HNO3 (65%)" and the carrier with the red dot.
QDR	Rinse in the Quick Dump Rinser with the standard program until the resistivity is 5 MΩ.
Drying	Use the Semitool "rinser/dryer" with the standard program, and the white carrier with a red dot.

11. MEASUREMENT

Use Keyence for measurement of deep holes in Si.

Wet etching of Oxide

12. Wet Etching Silicon oxide: 500nm (Etching line -- Si bath)

Moisten	Rinse for 1 minute in wet bench "H2O/Triton X-100 tbv BHF 1:7". Use the carrier with the blue dot. The bath contains 1 ml Triton X-100 per 5000 ml deionized water.
Etch	Use wet bench "BHF 1:7 (SiO2-ets) Si" at ambient temperature, and the carrier with the blue dot. The bath contains a buffered HF solution.
Time	Etch until the windows on the front side are hydrophobic, plus an extra 30 seconds. The required etch time depends on the layer thickness and composition. The etch rate of thermally grown oxide is 1.3 ± 0.2 nm/s at 20 °C.
Rinse	Rinse in the Quick Dump Rinser with the standard program until the resistivity is 5 MΩ.

Dry	Use the "Avenger Ultra-Pure 6" rinser/dryer with the standard program, and the white carrier with a black dot.
Inspection	Visually, through a microscope: All the windows must be open and the hydrophobic test may be applied.

13. CLEANING: HNO3 99% and 69.5%

Cleaning	10 minutes in fuming nitric acid (Merck: HNO3 100%) at ambient temperature. Use wet bench "HNO3 (100%) green metls" and the carrier with the red dot.
QDR	Rinse in the Quick Dump Rinser with the standard program until the resistivity is 5 MΩ.
Cleaning	10 minutes in concentrated nitric acid (Merck: HNO3 65%) at 110 °C. Use wet bench "HNO3 (65%)" and the carrier with the red dot.
QDR	Rinse in the Quick Dump Rinser with the standard program until the resistivity is 5 MΩ.
Drying	Use the Semitool "rinser/dryer" with the standard program, and the white carrier with a red dot.

Teflon coating

14. Teflon coating

Use the Rapier Omega i2L DRIE etcher and use recipe **'1FCdepo'**.
Follow the operating instructions from the manual when using this machine.

Number of cycles depend on the etching depth.

PDMS

START PDMS IN POLYMER LAB

15. PDMS PREPARATION

In this step the preparation of the PDMS will be done using the elastomer PDMS Sylgard 184 and its curing agent.

Pour 10 g of the PDMS elastomer in the disposable cup and 1 g of curing agent by using a pipette. Depending on the number of wafers to be processed these amounts could vary but the ratio between the elastomer and curing agent must be keep on 10:1.

Don't forget protecting the weighting machine of any leakage of elastomer or curing agent during the preparation of the material. Use for this a towel to protect the plate of the machine.

16. PDMS MIXING AND DEGASING

For mixing the PDMS elastomer and curing agent use the Thinky Speedmixer. Make sure that the cup holder is properly located in the machine. Determine the total weight of the cup and the holder and adjust the machine according to this value. Follow the instructions established for this machine.

Select program 01, check the parameters for each step if necessary and then start the process.

17. PDMS SPIN-COATING

18. BACKSIDE AND FRONTSIDE PDMS CLEANING (edges mostly)

Leave the wafer in the Lanz coater with vacuum on.
Use a cotton swab soaked in Acetone for cleaning the wafer backside and the frontside edge. Remove the PDMS from the edge of the wafer at least 4 mm deep towards the center of the wafer to avoid particles on the edge of the wafer.
Check also the backside of the wafer and remove any residual.

Note: Residuals are not allowed neither on the frontside nor the backside of the wafer.

19. Degassing

20. PDMS BAKING

For baking of the PDMS layer use the Memmert Oven with the dedicated carrier (PDMS). Set the temperature level to 90 °C. Establish the temperature level prior to this step since it takes some time because the heat capacity if the oven is high.

Bake the PDMS layer at 90 °C for 60 min.

Note: Check again at the end of the processing if any residual is present. Residuals are not allowed neither on the frontside nor the backside of the wafer.

END PDMS IN POLYMER LAB

21. INSPECTION PDMS RESIDUES

Visually inspect the wafers through a microscope, and check if the wafers are clean. No resist or PDMS residues are allowed

22. PEELING OFF PDMS